

## Metal-Organic Frameworks | Very Important Paper |

## VIP A Porous Zirconium-Based Metal-Organic Framework with the Potential for the Separation of Butene Isomers

Huimin Liu,<sup>[a]</sup> Yabing He,<sup>\*[a]</sup> Jingjing Jiao,<sup>[a]</sup> Dongjie Bai,<sup>[a]</sup> De-li Chen,<sup>[b]</sup> Rajamani Krishna,<sup>\*[c]</sup> and Banglin Chen<sup>\*[a, d]</sup>

**Abstract:** By using a novel  $C_3$ -symmetrical tricarboxylate ( $4,4',4''$ -benzene-1,3,5-triyl-1,1',1''-trinaphthoic acid), a novel zirconium-based metal-organic framework **ZJNU-30** was solvothermally synthesized and structurally characterized. Single-crystal X-ray structural analyses show that **ZJNU-30** consists of  $Zr_6$ -based nodes connected by the organic linkers to form a (3,8)-connected network featuring the coexistence of two different polyhedral cages: octahedral and cubooctahedral cages with the dimensions of about 14 and 22 Å, respectively. Remarkably, **ZJNU-30** is very stable when exposed to air for one month. More importantly, with a moderately

high surface area, hierarchical pore structures, and an aromatic-rich pore surface in the framework, **ZJNU-30**, after activation, exhibits a promising potential for the selective adsorptive separation of industrially important butene isomers consisting of *cis*-2-butene, *trans*-2-butene, 1-butene, and *iso*-butene at ambient temperature. This separation was established exclusively by gas adsorption isotherms and simulated breakthrough experiments. To the best of our knowledge, this is the first study investigating porous metal-organic frameworks for butene-isomer separation.

## Introduction

Metal-organic frameworks (MOFs), also known as porous coordination polymers (PCPs), are hybrid porous solids built up from inorganic metal ion subunits connected by polytopic organic ligands. MOFs have attracted great interest in the past couple of decades due to their intriguing characteristics like high porosities, tunable structures, and easily functionalized pore surfaces. These properties have afforded excellent application potentials in a variety of fields including, but not limited to, gas storage,<sup>[1]</sup> gas separation,<sup>[2]</sup> heterogeneous catalysis,<sup>[3]</sup> luminescent sensors,<sup>[4]</sup> proton conduction,<sup>[5]</sup> and drug delivery.<sup>[6]</sup> It is well known that these applications of MOFs mainly hinge on their porosities and stabilities. In terms of porosities,

a very wide range of MOFs with various pore sizes ranging from ultramicropore to mesopore have been realized due to the richness and variety of both metal ions and organic ligands constituting MOFs. In particular, remarkable breakthroughs in the construction of MOFs with ultrahigh porosities have been made, and several landmark MOFs displaying large experimental surface areas with values exceeding  $5000\text{ m}^2\text{ g}^{-1}$  have been reported; these include PCN-68,<sup>[7]</sup> UCMC-2,<sup>[8]</sup> MOF-210,<sup>[9]</sup> DUT-32,<sup>[10]</sup> and NU-110E.<sup>[11]</sup> Despite the important progress on the porosity, one significant limitation for the use of the overwhelming majority of MOF materials in practical applications is the poor hydrolytic stability under humidity. Generally, for practical use, an unstable material even with superior performance is much less cost-effective than the one that may have inferior performance but is more robust. Consequently, how to design and synthesize porous MOF materials with enhanced hydrolytic stability is still nowadays one of the key challenges for the MOF community.

The hydrostability of a given framework largely depends on its metal-ligand interaction holding the metal ions and organic linkers together, where the metal-containing clusters are often susceptible to attack by water molecules. Naturally, according to the HSAB (Hard and Soft Acids and Bases) principle suggested by Pearson, an efficient strategy to improve the hydrostability of an MOF is combining high-valence metal ions ( $Zr^{4+}$ ,  $Cr^{3+}$ ,  $Fe^{3+}$ ,  $Al^{3+}$ , etc.) with carboxylates to strengthen the metal-ligand coordination bonds.<sup>[12]</sup> This has been well demonstrated by the first Zr-based MOF UiO-66 (UiO stands for University of Oslo) built up from  $Zr_6O_4(OH)_4$  and benzenedicarboxylate linkers, first discovered by Cavka et al. in 2008.<sup>[12a]</sup> This first Zr-based MOF displays exceptionally good chemical

[a] H. Liu, Prof. Dr. Y. He, J. Jiao, D. Bai, Prof. Dr. B. Chen  
College of Chemistry and Life Sciences, Zhejiang Normal University  
Jinhua 321004 (China)  
E-mail: heyabing@zjnu.cn

[b] Dr. D.-L. Chen  
Key Laboratory of the Ministry of Education for Advanced Catalysis  
Materials Institute of Physical Chemistry, Zhejiang Normal University  
Jinhua 321004 (China)

[c] Prof. Dr. R. Krishna  
Van't Hoff Institute for Molecular Sciences, University of Amsterdam  
Science Park 904, 1098 XH Amsterdam (The Netherlands)  
E-mail: r.krishna@contact.uva.nl

[d] Prof. Dr. B. Chen  
Department of Chemistry, University of Texas at San Antonio  
One UTSA Circle, San Antonio, Texas 78249-0698 (USA)  
E-mail: banglin.chen@utsa.edu

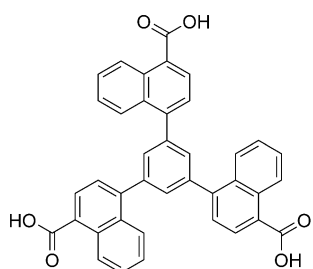
Supporting information and the ORCID number(s) for the author(s) of this article can be found under <http://dx.doi.org/10.1002/chem.201602892>.

resistance toward water compared to the majority of the other common MOFs. In addition, other successful strategies adopted to enhance the water stability of MOFs include the introduction of hydrophobic groups close to the coordinated metal centers,<sup>[13]</sup> and PDMS-coating treatment.<sup>[14]</sup> In this context, we turned our attention to Zr-cluster-based MOFs to develop highly stable and porous MOF materials for specialized applications.

Surprisingly, among the reported Zr-based MOFs, organic ligands are limited to dicarboxylate<sup>[15]</sup> and tetracarboxylate ligands,<sup>[16]</sup> whereas the Zr-MOFs based on tricarboxylate linkers have seldom been explored.<sup>[17]</sup> To the best of our knowledge, only two Zr-based MOFs based on tricarboxylate ligands were reported in the literature. One is built from the triangular BTC linker (benzene-1,3,5-tricarboxylate),<sup>[17a]</sup> whereas another is constructed from the expanded triangular BTB linker (4,4',4''-benzene-1,3,5-triyl-tribenzoate).<sup>[17b]</sup> Considering that extensive research has shown the use of  $C_3$ -symmetric tritopic carboxylate linkers is very useful in constructing porous MOF materials,<sup>[18]</sup> more Zr-based MOFs constructed from tricarboxylate need to be developed.

On the other hand, the separation of unsaturated olefins and dienes from C<sub>4</sub> hydrocarbon mixtures is very important in petrochemical processing. Due to the similar boiling points (*iso*-butane = 261.45 K; *iso*-butene = 266.25 K; 1-butene = 266.85 K; 1,3-butadiene = 268.75 K; *n*-butane = 272.65 K; *trans*-2-butene = 273.45 K; *cis*-2-butene = 276.85 K), the separation of C<sub>4</sub> streams to recover the valuable 1,3-butadiene, 1-butene, and *iso*-butene by distillation is very difficult and energy-intensive. Appropriately designed MOFs offer energy-efficient alternatives for the separation of C<sub>4</sub> hydrocarbons.

In this study, we report the solvothermal synthesis of a novel Zr-MOF designed as **ZJNU-30** (ZJNU: Zhejiang Normal University) based on Zr<sub>6</sub> clusters and a  $C_3$ -symmetrical trigonal tricarboxylate linker, 4,4',4''-benzene-1,3,5-triyl-1,1',1''-trinaphthoic acid (H<sub>3</sub>L, Scheme 1). A multi-tier approach was used to examine the potential of **ZJNU-30** for the separation of C<sub>4</sub> hydrocarbon mixtures; this strategy consists of a combination of experimental data on unary isotherms, ideal adsorbed solution theory (IAST) calculations, and simulated breakthrough experiments. We aimed to demonstrate that **ZJNU-30** has good potential for the separation of butene mixtures; this is the first publication to demonstrate the potential of porous MOFs for this challenging separation.



Scheme 1. The chemical structure of the organic linker H<sub>3</sub>L used to construct **ZJNU-30**.

## Results and Discussion

### Synthesis and characterization

The organic ligand, 4,4',4''-benzene-1,3,5-triyl-1,1',1''-trinaphthoic acid, was readily synthesized by a Suzuki cross-coupling reaction of 1,3,5-tribromobenzene and methyl 4-(pinacolboryl)-1-naphthalate followed by hydrolysis and acidification, providing a good yield (see the Experimental Section for details). Its chemical structure was characterized by <sup>1</sup>H and <sup>13</sup>C NMR, and FTIR spectroscopies. Solvothermal reaction of the organic linker with anhydrous ZrCl<sub>4</sub> in *N,N*-dimethyl acetamide (DMA) at 403 K for 86 h in the presence of benzoic acid as modulator resulted in the formation of octahedron-shaped colorless crystals of **ZJNU-30** in a decent yield (32%). The crystals were not soluble in common solvents such as DMF (*N,N*-dimethylformamide), DMA, 1,4-dioxane, THF, MeOH, EtOH, acetone, CH<sub>2</sub>Cl<sub>2</sub>, and CHCl<sub>3</sub>. The structure of **ZJNU-30** was determined by single-crystal X-ray diffraction, and the phase purity of the bulk material was confirmed by a good match of the powder X-ray diffraction (PXRD) pattern with the simulated one calculated from the single-crystal X-ray structure (see Figure 2a). Based on the single-crystal X-ray diffraction structural determination, thermogravimetric analysis (TGA, Figure S1 in the Supporting Information), and elemental analysis, **ZJNU-30** can be best formulated as [Zr<sub>9</sub>O<sub>6</sub>(OH)<sub>6</sub>(PhCOO)<sub>6</sub>(L)<sub>4</sub>]·24 DMA.

### Structural description

Single-crystal X-ray analysis revealed that **ZJNU-30** crystallized in the cubic space group of Pm-3m with  $a = 28.345(5)$  Å. In addition to guest molecules, the asymmetric unit comprises three-eighths of Zr<sup>4+</sup> ions, one-sixth of fully deprotonated ligands, one-fourth of benzoate, one-fourth of  $\mu_3$ -oxo atoms and one-fourth of  $\mu_3$ -hydroxyl groups. The coordination geometry of the Zr<sup>4+</sup> ion can be described as a square-antiprism consisting of eight oxygen atoms. As found in most Zr-based MOFs,<sup>[19]</sup> the basic inorganic secondary building unit in **ZJNU-30** is the octahedral Zr<sub>6</sub> cluster Zr<sub>6</sub>O<sub>4</sub>(OH)<sub>4</sub>(COO)<sub>12</sub>, in which each Zr<sup>4+</sup> occupies the vertex of an octahedron and the triangular faces are alternatively capped by  $\mu_3$ -O and  $\mu_3$ -OH groups. However, unlike the well-known 12-connected Zr<sub>6</sub> clusters observed in UiO-66 series of MOFs,<sup>[12a]</sup> only eight edges of the Zr<sub>6</sub> octahedron are bridged by carboxylates from L<sup>3-</sup> ligands, whereas the remaining positions are occupied by the terminal benzoate involved in the MOF synthesis protruding towards the channels. The octahedral cores are further connected by the tritopic organic linkers to give rise to an extended three-dimensional network. The interesting structural characteristic is a hierarchical combination of microporous octahedral and mesoporous cuboctahedral cages, as well as the coexistence of cages and channels in the framework (Figure 1e). Octahedral cages are formed by six Zr<sub>6</sub> clusters occupying the vertices connected by eight organic ligands covering the faces, as shown in Figure 1c. In contrast, the cuboctahedral cages are formed by twelve Zr<sub>6</sub> clusters occupying the vertices connected by eight organic ligands covering the triangular faces, as

shown in Figure 1 d. The diameters of octahedral and cuboctahedral cages are about 14 and 22 Å, taking into account the van der Waals radii of the atoms. Each cuboctahedral cage is surrounded by eight octahedral cages through the sharing of the triangular faces and vice versa. Cuboctahedral cages are interconnected by four-membered windows to form one-dimensional infinite channels running along each crystallographical-axis direction. There are two different types of windows separating these cages, which allow the guest molecules to access the inner pore system. The total solvent-accessible volume is 63.8% of the volume of the unit cell when the disordered solvent molecules are removed ( $14\,522.2\text{ }\text{\AA}^3$  out of the  $22\,773.5\text{ }\text{\AA}^3$  per unit cell volume), calculated using the PLATON routine.<sup>[20]</sup>

For topological analysis, the  $\text{Zr}_6$  core is connected by eight organic ligands and can be regarded as an 8-connected node (Figure 1 a), whereas each organic ligand links to three  $\text{Zr}_6$  cores and therefore can be treated as a 3-connected node (Figure 1 b). Thus, the overall network can be simplified to a (3,8)-connected net with Schläfli symbol of  $\{4^8\cdot6^4\cdot8^{12}\cdot10^4\}$ , as indicated by TOPOS software (Figure S2 in the Supporting Information). Notably, **ZJNU-30** adopts a topology different from that of two reported Zr-tricarboxylate frameworks. MOF-808 based on the BTC linker has a (6,3)-connected three-dimensional framework with an overall **spn** topology,<sup>[17a]</sup> whereas the Zr-MOF based on the BTB linker is a two-dimensional network adopting a **kgd** topology.<sup>[17b]</sup>

### Permanent porosity

To assess the permanent porosities, the  $\text{N}_2$  adsorption-desorption isotherm was collected at 77 K by using a Micromeritics ASAP 2020 HD88 surface-area-and-pore-size analyzer. Prior to gas sorption measurements, the as-synthesized sample **ZJNU-30** was washed with copious amount of DMA and then solvent-exchanged with dry acetone, followed by the evacuation under a dynamic vacuum at 373 K for 24 h, generating the activated **ZJNU-30a** (thereafter, “a” represents the activated form of MOF materials). Retention of the framework structure after activation was confirmed by X-ray diffraction (Figure 2 a). As shown in Figure 2 b, **ZJNU-30a** displays a reversible pseudo-type-I adsorption isotherm showing changes of slopes at relatively low pressures, which is consistent with the presence of different pore geometries within the structure. Based on the  $\text{N}_2$  adsorption isotherm, the Brunauer-Emmett-Teller (BET, considering the consistency criteria proposed by Rouquerol and Llewellyn<sup>[21]</sup>) and Langmuir surface areas were calculated to be 1570 and  $3298\text{ m}^2\text{ g}^{-1}$ , respectively (Figure S3 in the Supporting Information).<sup>[22]</sup> The pore volume calculated from the maximum amount of  $\text{N}_2$  adsorbed is  $1.15\text{ cm}^3\text{ g}^{-1}$ , which is in good agreement with the calculated value of  $1.07\text{ cm}^3\text{ g}^{-1}$  using PLATON software<sup>[20]</sup> and is also among the highest values ever reported for the Zr-based MOFs (Table S1 in the Supporting Information). The mean pore sizes obtained from the NLDFT (non-local density functional theory) model are predominantly around 1.36 and 2.16 nm (the inset in Figure 2 b), which are close to the sizes of octahedral and cuboctahedral cages determined from the crystal structure.

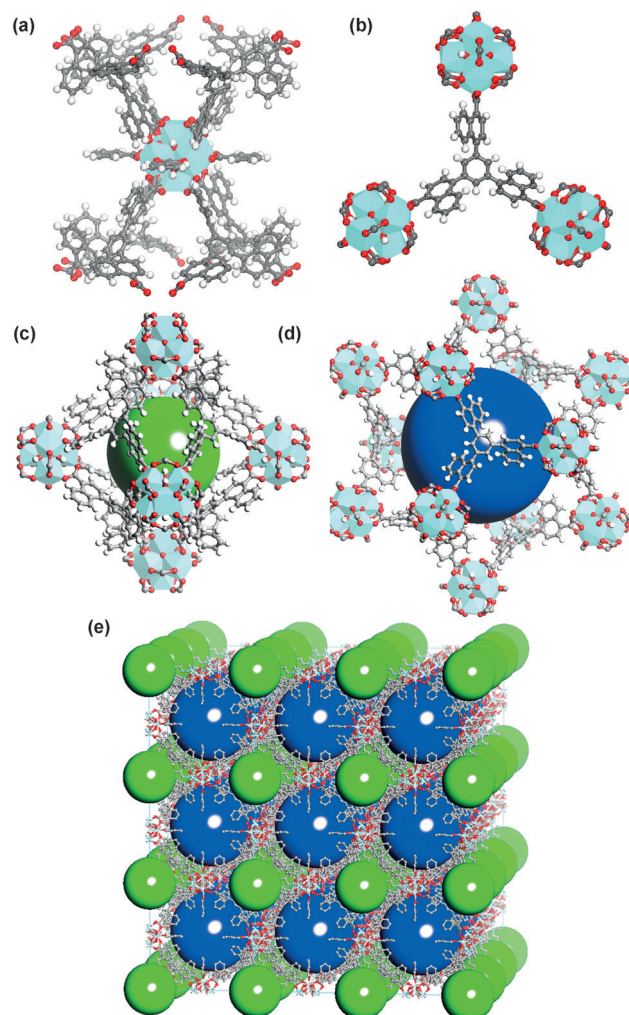


**Figure 1.** Single-crystal X-ray structure of **ZJNU-30** showing that a) each  $\text{Zr}_6$  cluster is connected to eight organic ligands and b) each organic ligand coordinates to three  $\text{Zr}_6$  clusters. The view of c) octahedral cages with an effective pore diameter of ca. 14 Å indicated by the green sphere, and d) cuboctahedral cages with an effective pore diameter of ca. 22 Å indicated by the blue sphere in **ZJNU-30**. e) A three-dimensional porous structure featuring the coexistence of two different types of pore cages.

### Thermal and hydrolytic stability

To assess the thermal stability, the TGA was carried out from room temperature to 1073 K under nitrogen atmosphere (Figure S1 in the Supporting Information). TGA reveals that **ZJNU-30** displays an obvious decline before 423 K, corresponding to the release of solvent molecules trapped in the pores. Thereafter, the solvent-free framework could be thermally stable up to 773 K, followed by the collapse upon further calcination. The thermally stability is comparable to that of UiO-66 and its analogues.<sup>[12a]</sup>

In addition to the thermal stability, the hydrothermal stability of **ZJNU-30** was also explored. The activated sample **ZJNU-30a** was exposed to air for one month, or immersed in water as well as aqueous solutions of 2 M HCl for one week at ambient temperature, and the PXRD patterns were then examined. No significant loss of crystallinity was observed for these treat-

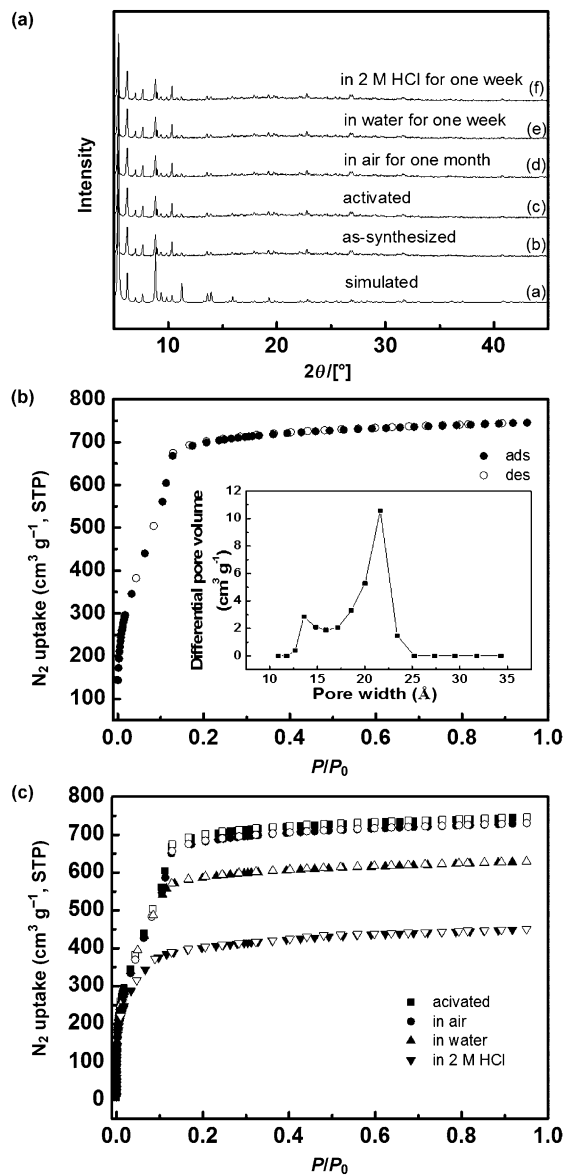


**Figure 2.** a) PXRD patterns and c)  $N_2$  adsorption–desorption isotherms at 77 K of the treated samples. b)  $N_2$  adsorption and desorption isotherms at ZJNU-30a at 77 K. Solid and open symbols represent adsorption and desorption, respectively. The inset: pore size distribution calculated by NLDFT method.

ed samples (Figure 2a). Considering that a small degradation of the framework is not visible in the PXRD pattern, we further measured the  $N_2$  adsorption isotherms of these treated samples at 77 K. Adsorption studies revealed that almost no loss in the amount of  $N_2$  adsorbed was observed when the activated sample was exposed to air for one month, whereas exposure of the activated sample in water or 2 M HCl for one week led to a certain reduction of the adsorption amount of  $N_2$  (Figure 2c), indicating the moderate hydrostability of the activated ZJNU-30a.

## Separation of butene isomers

A C<sub>4</sub> hydrocarbon fraction obtained from various hydrocarbon cracking operations consists of *n*-butane, *iso*-butane, *iso*-butene, 1-butene, *cis*-2-butene, *trans*-2-butene, and 1,3-butadiene. The most valuable components in C<sub>4</sub> hydrocarbons are *iso*-butene, 1-butene, and 1,3-butadiene. For example, *iso*-butene is an important building block for many valuable products such as *tert*-butyl alcohol, methyl *tert*-butyl ether, methyl methacrylate, and 1-*tert*-butyl-4-methylbenzene. 1-butene is used as a monomer feedstock in the production of poly(1-butene), or as co-monomer in the production of linear low density polyethylene (LLDPE). Also, 1-butene is converted into various fine chemicals such as sec-butanol and methyl ethyl ketone. 1,3-Butadiene is used to produce synthetic rubbers (butadiene homopolymers, styrene-butadiene rubber or nitrile rubber), which are used in a wide variety of consumer and industrial products that provide tremendous benefit to society. As such, the separation of C<sub>4</sub> streams to recover the valuable 1,3-butadiene, 1-butene, and *iso*-butene is an important way to increase the added value. Because their physicochemical properties such as volatility and boiling point are very similar, the separation of C<sub>4</sub> streams by simple distillation is a highly energy-intensive process in the chemical industry. Among the many alternatives considered, physisorption-based processes involving porous adsorbents that are able to discriminate C<sub>4</sub> hydrocarbons are of great interest.<sup>[23]</sup> A few zeolites and  $\pi$ -complexation adsorbents have been examined for such a separation.<sup>[24]</sup> For example, Palomino et al. reported that it is possible to perform the kinetic separation of *trans*-2-butene and 1-butene from the C<sub>4</sub> fraction by using pure silica ITQ-32 zeolite as adsorbent.<sup>[24c]</sup> Tijsebaert et al. have demonstrated the potential of the all-silica zeolite RUB-41 for liquid phase separation of *cis*-2-butene and *trans*-2-butene from 1-butene.<sup>[24a]</sup> Yang et al. investigated the feasibility of using the  $\pi$ -complexation sorbents (AgY<sup>[24f]</sup> and CuY<sup>[24d]</sup> zeolites) to effectively remove trace amounts of butadiene from 1-butene, but the issue related to long-term operation needs to be considered. Given the fact that compared to zeolites, the MOFs have some unique features such as high porosities, tunable pore sizes, and functionalizable pore surfaces, there is a need to explore porous MOFs for such a purpose.

ZJNU-30a does not have Lewis acidic uncoordinated metal sites that are accessible, which avoids olefin oligomerization that will lead to pore blocking after prolonged time. It also exhibits high porosity, which facilitates the diffusion of large-sized gas molecules into the pores. Considering these properties, we investigated the potential of ZJNU-30a for the separation of C<sub>4</sub> hydrocarbon mixtures. Accordingly, the equilibrium adsorption isotherms of *n*-butane, *iso*-butane, 1-butene, *cis*-2-butene, *trans*-2-butene, *iso*-butene, and 1,3-butadiene were measured systematically at three different temperatures of 288 K, 298 K, and 308 K up to 1 atm. As expected, diffusion of all C<sub>4</sub> hydrocarbons in ZJNU-30a is fast because the measurement of each adsorption isotherm was completed in 5 h (equilibrium time: 25 s when  $P < 30 \text{ mmHg}$ , and 5 s when  $P = 30\text{--}1000 \text{ mmHg}$ ). There is almost no observable loss in the ad-

sorbed amount after five consecutive cycles (Figure S4 in the Supporting Information; note that the reactivation process was applied between each cycle, which was achieved by heating the sample at 333 K until the degassed rate reached  $3 \mu\text{mHg min}^{-1}$ ), indicating the gas sorption isotherms are reproducible, and the polymerization of butene and butadiene during the adsorption was not observed. As shown in Figure 3, all isotherms, except those for *iso*-butene and 1,3-butadiene at 308 K, reach the saturation as the pressure increases to 1 atm, and display a remarkable hysteresis upon desorption. The sorption hysteresis existing between adsorption and desorption branches of the isotherms can be interpreted as follows: the large-sized  $\text{C}_4$  hydrocarbon adsorbate molecules have comparable sizes with the window, hindering them to escape from the pore upon desorption. Interestingly, two distinct steps were found in the adsorption isotherms. Due to the framework remaining intact after activation, the possibility of the structural transition of the MOF to be the origin of the stepped isotherms, as demonstrated in flexible ZIF-7,<sup>[25]</sup> is ruled out. We tentatively attributed the stepped isotherms to sequential filling of  $\text{C}_4$  hydrocarbons into two distinct cages in the framework. Similar adsorption behaviors were also observed in the previous study for alkanes in MOFs with hierarchical cages such as HKUST-1.<sup>[26]</sup> The sorption isotherms for each adsorptive exhibit the expected temperature dependence for loadings, that is, the lower the measurement temperature, the higher the excess amount of the respective hydrocarbons. It should be mentioned that in the report by Palomino et al.,<sup>[24c]</sup> the uptake of these gases increases with the temperature, which the authors think is attributed to the strong diffusional restrictions. Due to the large pore volume, **ZJNU-30a** adsorbs a large amount of  $\text{C}_4$  hydrocarbons. The adsorbed amounts of *cis*-butene, *n*-butane, *trans*-2-butene, 1-butene, *iso*-butane, 1,3-butadiene, and *iso*-butene of **ZJNU-30a** at 298 K and 1 atm are 282, 265, 249, 240, 236, 238, and  $205 \text{ cm}^3 \text{ g}^{-1}$  at STP (standard temperature and pressure), respectively. This corresponds to 102.8, 96.6, 90.7, 87.5, 86.0, 86.8, and 74.7 molecules adsorbed per unit cell, respectively, which reflects differences in the efficiencies by which the  $\text{C}_4$  hydrocarbons pack themselves within the pore. The better packing efficiency for a linear isomer than a branched isomer might be due to the effect of configurational entropy, which is similar with that observed in IRMOF-13, IRMOF-14, PCN-6', and PCN-6,<sup>[27]</sup> but different with that observed in IRMOF-1 and IRMOF-6, in which the amounts of adsorbed branched alkanes is larger than that of the linear ones.<sup>[28]</sup> When the temperature decreased to 288 K, the amounts of adsorbed *cis*-butene, *n*-butane, *trans*-2-butene, 1-butene, *iso*-butane, 1,3-butadiene, and *iso*-butene increased to 291, 277, 266, 252, 246, 259, and  $221 \text{ cm}^3 \text{ g}^{-1}$  (STP), respectively. These values are significantly higher than those of conventional adsorbents like activated carbons and zeolites.<sup>[24a,d,e,29]</sup> It should be mentioned that the experimental data on the adsorption of  $\text{C}_4$  hydrocarbons, in particular *cis*-2-butene, *trans*-2-butene, and 1,3-butadiene, on MOFs are extremely limited to date. A detailed comparison of  $\text{C}_4$ -hydrocarbon adsorption capacities of **ZJNU-30a** with those of other reported MOF materials is presented in Table S2 in the Supporting Information. It

can be observed that the sorption capacities of **ZJNU-30a** for  $\text{C}_4$ -hydrocarbons are relatively high compared to some other MOF materials under the similar conditions, and butane adsorption capacity is only surpassed by DUT-6(Zn) so far.

To check whether **ZJNU-30a** can separate  $\text{C}_4$  mixtures, we performed IAST and simulated breakthrough calculations. The experimentally measured loadings for *n*-butane, *iso*-butane, 1-butene, *iso*-butene, *cis*-2-butene, *trans*-2-butene, and 1,3-butadiene at temperatures of 288, 298, and 308 K in **ZJNU-30a** were fitted with the dual-site Langmuir-Freundlich isotherm (DSLF) model (Figure S5 in the Supporting Information). The fitting parameters provided in Table S3 in the Supporting Information, were then used to perform the corresponding calculations. Figure 4a presents the IAST calculations of uptake capacities of each component for adsorption from an equimolar seven-component mixture of *n*-butane, *iso*-butane, 1-butene, *iso*-butene, *cis*-2-butene, *trans*-2-butene, and 1,3-butadiene, in **ZJNU-30a** at 298 K. At a total pressure of 100 kPa, we obtain the hierarchy of component loadings as follows: *cis*-2-butene > *n*-butane > *trans*-2-butene > 1-butene > *iso*-butane > 1,3-butadiene > *iso*-butene. From the component loadings calculated using IAST, we can determine the *n*-butane/*iso*-butane ( $n\text{C}_4/\text{iC}_4$ ), *cis*-2-butene/*trans*-2-butene, and 1-butene/*iso*-butene selectivities at 298 K as a function of pressure; these are presented in Figure 4b. The selectivities are in the range of 1.5–2 over the entire range of pressures, which are not as high as expected. The 1-butene/*iso*-butene selectivity is slightly better than that of IRMOF-1.<sup>[28]</sup>

The separation characteristic of an adsorbent is determined not only by the adsorption selectivity, but also more importantly by the uptake capacity. To appropriately evaluate the combined effects of adsorption selectivity and uptake capacity, we carried out transient breakthrough simulations using the simulation methodology described in the literature.<sup>[30]</sup> For the breakthrough simulations, the following parameter values were used: length of packed bed,  $L = 0.3 \text{ m}$ ; voidage of packed bed,  $\varepsilon = 0.4$ ; superficial gas velocity at inlet,  $u = 0.04 \text{ m s}^{-1}$ . The framework density of **ZJNU-30a** is  $596 \text{ kg m}^{-3}$ . Figure 4c presents transient breakthrough simulations for the separation of an equimolar seven-component mixture of *n*-butane, *iso*-butane, 1-butene, *iso*-butene, *cis*-2-butene, *trans*-2-butene, and 1,3-butadiene in **ZJNU-30a** at 298 K, each with a partial pressure of 12 kPa. We note that the hierarchy of breakthrough times is *cis*-2-butene > *n*-butane > *trans*-2-butene > 1-butene > *iso*-butane > 1,3-butadiene > *iso*-butene, which is a precise reflection of the hierarchy of component loadings in Figure 4a. However, there is overlap in the breakthroughs, and it appears that it is not possible to separate each of these mixtures in a nearly pure form.

From the results in Figure 4c, it appears that **ZJNU-30a** is most suited to the separation of 1-butene/*iso*-butene/*cis*-2-butene/*trans*-2-butene mixtures. To demonstrate this, Figure 5a shows IAST calculations of uptake capacities of each component for adsorption from an equimolar four-component 1-butene/*iso*-butene/*cis*-2-butene/*trans*-2-butene mixture in **ZJNU-30a** at 298 K. At a total pressure of 100 kPa, we obtain the following hierarchy of component loadings: *cis*-2-butene >

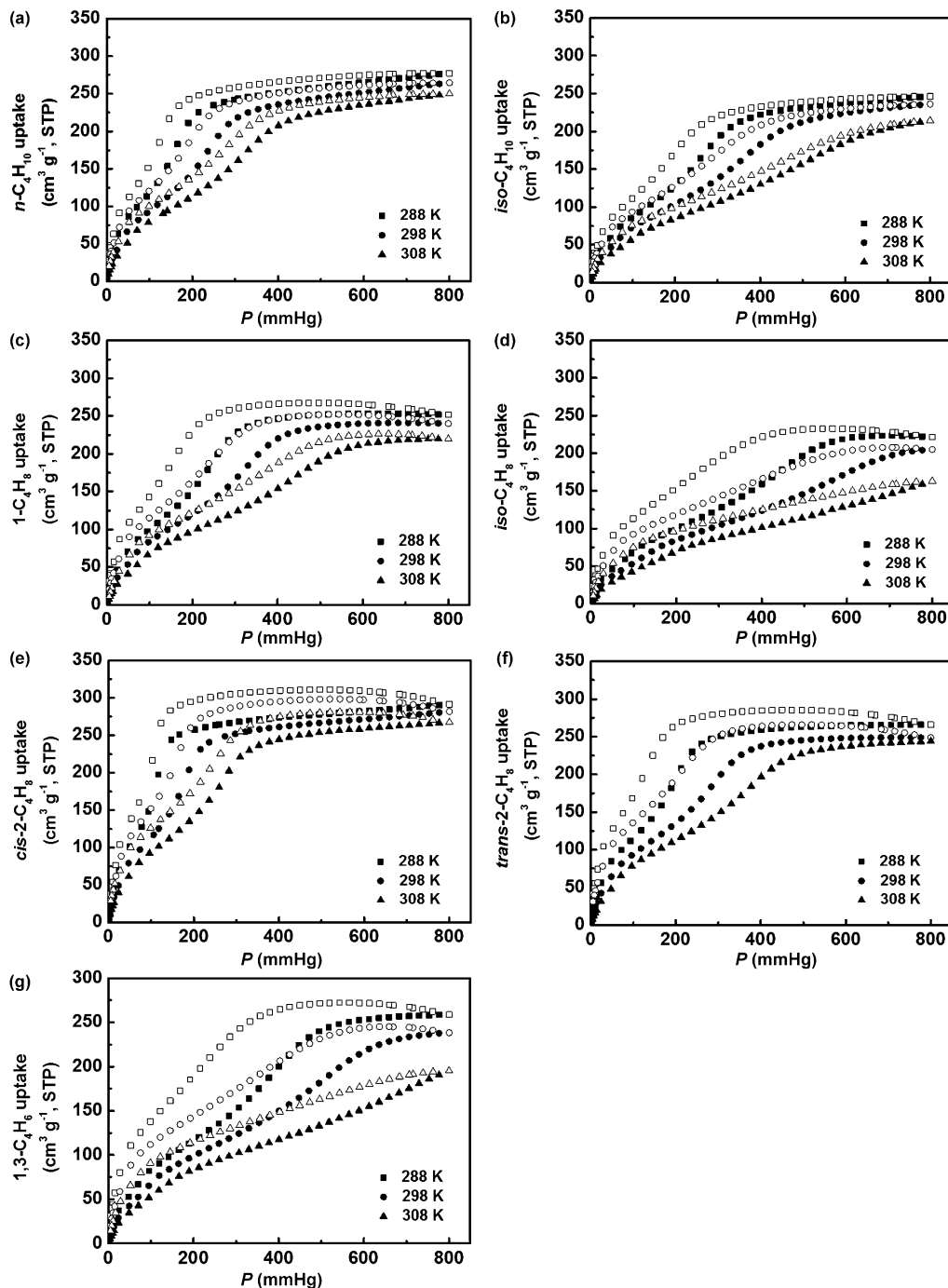


**Figure 3.** Adsorption isotherms of *n*-butane (a), *iso*-butane (b), 1-butene (c), *iso*-butene (d), *cis*-2-butene (e), *trans*-2-butene (f), and 1,3-butadiene (g) in **ZJNU-30a** at 288, 298, and 308 K. Solid and open symbols correspond to adsorption and desorption, respectively.

*trans*-2-butene > 1-butene > *iso*-butene. On the basis of the IAST calculations, we expect the separation of a mixture of butene isomers is sharper. To verify this expectation, Figure 5 b depicts transient breakthrough simulations for the separation of an equimolar four-component 1-butene/*iso*-butene/*cis*-2-butene/*trans*-2-butene mixture in **ZJNU-30a** at 298 K, each with a partial pressure of 25 kPa. We note that the hierarchy of breakthrough times is *cis*-2-butene > *trans*-2-butene > 1-butene > *iso*-butene, which is a precise reflection of the hierarchy of component loadings in Figure 5 a. We note clear separa-

tions between *cis*-2-butene and *trans*-2-butene, and between 1-butene and *iso*-butene, demonstrating that **ZJNU-30a** has good potential for separation of 1-butene/*iso*-butene/*cis*-2-butene/*trans*-2-butene mixtures. Further experiments are ongoing to confirm this promising separation potential.

## Conclusions

In summary, we synthesized a new tricarboxylate ligand and employed it to construct (3,8)-connected Zr-based MOF **ZJNU-**

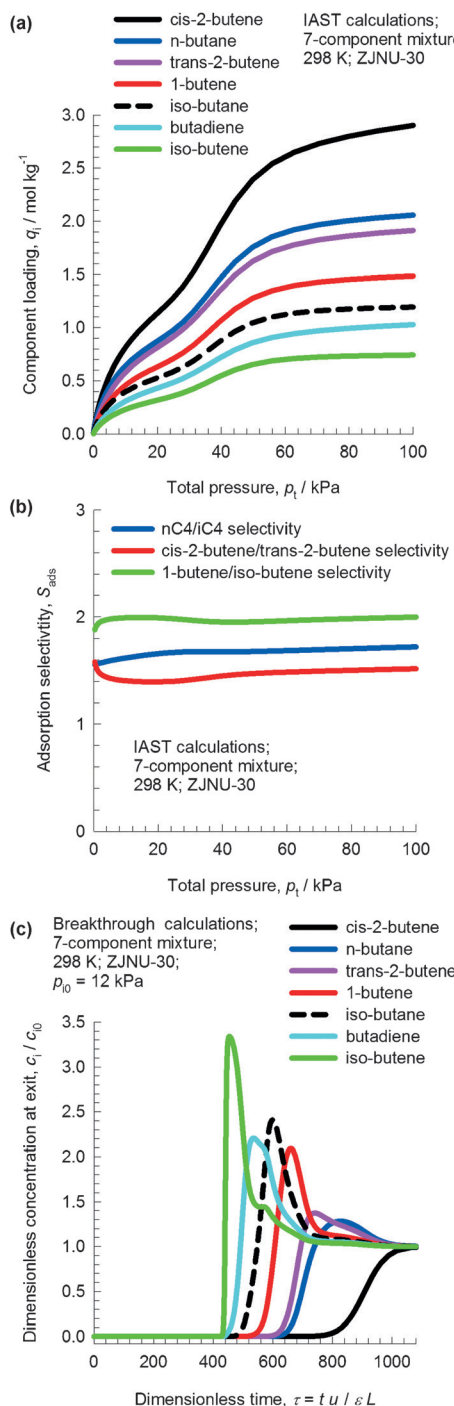


**Figure 4.** a) IAST calculations of uptake capacities of each component for adsorption from an equimolar seven-component mixture of *n*-butane, *iso*-butane, 1-butene, *iso*-butene, *cis*-2-butene, *trans*-2-butene, and 1,3-butadiene, in **ZJNU-30a** at 298 K; b) IAST calculations of nC4/iC4, *cis*-2-butene/*trans*-2-butene, and 1-butene/*iso*-butene selectivities for adsorption from an equimolar seven-component mixture of *n*-butane, *iso*-butane, 1-butene, *iso*-butene, *cis*-2-butene, *trans*-2-butene, and 1,3-butadiene in **ZJNU-30a** at 298 K; and c) transient breakthrough simulations for the separation of an equimolar seven-component mixture of *n*-butane, *iso*-butane, 1-butene, *iso*-butene, *cis*-2-butene, *trans*-2-butene, and 1,3-butadiene in **ZJNU-30a** at 298 K, each with a partial pressure of 12 kPa.

30, featuring the coexistence of two different types of cages: octahedral and cuboctahedral cages in the framework. The

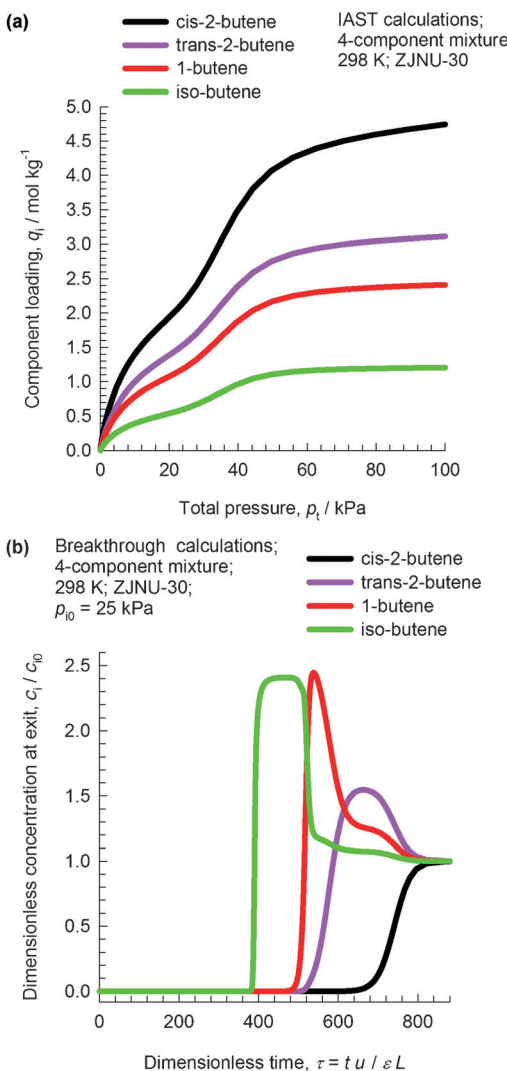


**Figure 5.** a) IAST calculations of uptake capacities of each component for adsorption from an equimolar four-component mixture of 1-butene/*iso*-butene/*cis*-2-butene/*trans*-2-butene in **ZJNU-30a** at 298 K, and b) transient breakthrough simulations for the separation of an equimolar 4-component mixture of 1-butene/*iso*-butene/*cis*-2-butene/*trans*-2-butene mixtures in **ZJNU-30a** at 298 K, each with a partial pressure of 25 kPa.

MOF shows the promising potential for the separation of butene isomer mixtures. The selective adsorptive separation might be mainly attributed to the unique pore characteristics as well as an aromatic-rich pore surface in **ZJNU-30a**. This is the first study investigating MOFs for butene isomer separation. This work will initiate more investigations on emerging MOFs for such an industrially important separation. Given that the pore sizes of MOFs can be tuned by the interplay of metal ions and organic linkers to enhance their size-selective separations, and the pore surface can be functionalized by the immobilization of specific sites to direct molecular recognition, extensive research on porous MOFs is expected to lead to the discovery of better materials that offer enhanced capacities for butene isomer separation in the near future.

## Experimental Section

**Materials and methods:** All chemicals were purchased from commercial sources and used as received unless otherwise noted.  $^1\text{H}$  and  $^{13}\text{C}$  NMR spectra of the compounds were measured using a Bruker AVANCE 400 or 600 NMR spectrometer by dissolving the samples in  $[\text{D}_6]\text{DMSO}$  or  $\text{CDCl}_3$ . The chemical shifts were reported in parts per million (ppm) with use of residual solvent as an internal standard for  $^1\text{H}$  ( $\delta(\text{CDCl}_3)=7.26$  ppm,  $\delta([\text{D}_6]\text{DMSO})=2.50$  ppm) and  $^{13}\text{C}$  spectra ( $\delta(\text{CDCl}_3)=77.16$  ppm,  $\delta([\text{D}_6]\text{DMSO})=39.52$  ppm). Fourier transform infrared (FTIR) spectra were recorded on a Nicolet 5DX FT-IR spectrometer with samples in KBr pellets in the range of 4000–400  $\text{cm}^{-1}$ . The elemental analysis of C, H, and N was performed on a Vario EL III CHNOS elemental analyser. TGA was performed on a Netzsch STA 449C thermal analyser with a heating rate of 5  $\text{K min}^{-1}$  in a flowing nitrogen atmosphere (10  $\text{mL min}^{-1}$ ). PXRD patterns were recorded on a Philips PW3040/60 automated powder diffractometer, using  $\text{Cu}_{\text{Ka}}$  radiation ( $\lambda=1.542 \text{ \AA}$ ) with a 2 $\theta$  range of 5–40°. An ASAP 2020 HD88 surface-area-and-pore-size analyser was used to volumetrically measure the adsorption behaviors. The sorption measurement was maintained at 77 K with liquid nitrogen and at other specified temperatures by a circulating bath (Julabo F12).

**Single-crystal X-ray crystallography:** The X-ray diffraction data were collected at 100(2) K on a Agilent supernova dual diffractometer with  $\text{Mo}_{\text{Ka}}$  radiation ( $\lambda=0.71073 \text{ \AA}$ ). The structure was solved by direct methods with SHELXS-97 and refined with a full-matrix least-squares technique within the SHELXL program package.<sup>[31]</sup> The unit cell includes a large region of disordered solvent molecules, which could not be modelled as discrete atomic sites. We employed PLATON/SQUEEZE<sup>[20]</sup> to calculate the diffraction contribution of the solvent molecules and, thereby, to produce a set of solvent-free diffraction intensities; structures were then refined again using the data generated. The crystal data and structure refinement results are listed in Table S4 in the Supporting Information. CCDC 1446516 (ZJNU-30) contains the supplementary crystallographic data for this paper. These data can be obtained free of charge from The Cambridge Crystallographic Data Centre.

## Synthesis and characterization of the organic linkers

**Methyl 4-bromo-1-naphthoate:** To 4-bromo-1-naphthoic acid (10.00 g, 39.83 mmol, Shanghai Shaoyuan Co. Ltd.) in methanol (280 mL), was added concentrated  $\text{H}_2\text{SO}_4$  (10 mL). The solution was refluxed for 24 h under a nitrogen atmosphere. After the solution was cooled to room temperature, the solvent was rotary-evaporated, and  $\text{CH}_2\text{Cl}_2$  (150 mL) and  $\text{H}_2\text{O}$  (150 mL) were added. The organic phase was separated and the aqueous phase was extracted with  $\text{CH}_2\text{Cl}_2$  (50 mL  $\times 2$ ). The organic phase was combined, washed with saturated  $\text{NaHCO}_3$  aqueous solution and brine subsequently, dried over anhydrous  $\text{MgSO}_4$ , and filtered. Removal of the volatile solvent gave the target compound (10.2 g, 38.5 mmol, 97%), which was pure enough for the next reaction.  $^1\text{H}$  NMR (400.1 MHz,  $\text{CDCl}_3$ ):  $\delta=8.94$ –8.98 (m, 1 H), 8.35–8.38 (m, 1 H), 8.03 (d,  $J=8.0$  Hz, 1 H), 7.86 (d,  $J=8.0$  Hz, 1 H), 7.67–7.70 (m, 2 H), 4.03 ppm (s, 3 H).

**Methyl 4-(4,4,5,5-tetramethyl-1,3,2-dioxaborolan-2-yl)-1-naphthoate:** methyl 4-bromo-1-naphthoate (11.00 g, 41.49 mmol), bis(pinacolato)diboron ( $\text{B}_2\text{Pin}_2$ , 11.59 g, 45.64 mmol, Beijing HWRK Chem Co.,Ltd.), KOAc (12.22 g, 124.48 mmol), and Pd(dppf) $\text{Cl}_2$  (0.91 g, 1.24 mmol, Beijing HWRK Chem Co.,Ltd.) were placed in a 500 mL flask equipped with a condenser for refluxing and a magnetic stirring bar. The flask was evacuated and refilled with  $\text{N}_2$ . The process was repeated three times, dry dioxane (250 mL) was then added using a syringe. The resulting mixture was stirred at 353 K

for 24 h. After the solvent was rotary-evaporated,  $\text{CH}_2\text{Cl}_2$  (200 mL) and  $\text{H}_2\text{O}$  (200 mL) were added. The organic phase was separated and the aqueous phase was extracted with  $\text{CH}_2\text{Cl}_2$  (80 mL  $\times 2$ ). The organic phase was combined, washed with brine (80 mL), dried over anhydrous  $\text{MgSO}_4$ , and filtered. After removal of the volatiles, the residue was purified using silica gel column chromatography (100–200 mesh, Qingdao Haiyang Chemical Co., Ltd) with petroleum ether/ethyl acetate (40/1, v/v) as eluent, affording the methyl 4-(4,4,5,5-tetramethyl-1,3,2-dioxaborolan-2-yl)-1-naphthoate as a white solid (10.6 g, 33.85 mmol, 81.6%).  $^1\text{H}$  NMR (400.1 MHz,  $\text{CDCl}_3$ ):  $\delta=8.81$ –8.86 (m, 2 H), 8.09–8.10 (m, 2 H), 7.58–7.64 (m, 2 H), 4.03 (s, 3 H), 1.46 ppm (s, 12 H).

**Trimethyl 4,4',4''-benzene-1,3,5-triyl-1,1',1''-trinaphthonate:** To a mixture of 1,3,5-tribromobenzene (1.90 g, 6.03 mmol, Beijing HWRK Chem Co.,Ltd.), methyl 4-(4,4,5,5-tetramethyl-1,3,2-dioxaborolan-2-yl)-1-naphthoate (6.78 g, 21.72 mmol),  $\text{K}_3\text{PO}_4$  (9.22 g, 43.42 mmol, Acros), and  $\text{Pd}(\text{PPh}_3)_4$  (1.05 g, 0.90 mmol, Beijing HWRK Chem Co.,Ltd.), was added dry dioxane (200 mL). The resulting mixture was stirred under reflux under a nitrogen atmosphere for 72 h. After removal of the solvents,  $\text{CH}_2\text{Cl}_2$  (100 mL) and  $\text{H}_2\text{O}$  (100 mL) were added. The mixture was filtered. The organic phase was separated and the aqueous phase was extracted with  $\text{CH}_2\text{Cl}_2$  (50 mL  $\times 2$ ). The combined organic phase was washed with brine (80 mL), dried over anhydrous  $\text{MgSO}_4$  and filtered. Volatiles were removed by rotary evaporation under reduced pressure, and the residue was purified by silica-gel column chromatography using petroleum ether/ $\text{CH}_2\text{Cl}_2$  (10/1, v/v) as eluent to give the tetramethyl intermediate as a white solid (2.89 g, 4.58 mmol, 76%).  $^1\text{H}$  NMR ( $\text{CDCl}_3$ , 400.1 MHz):  $\delta=9.03$  (d,  $J=8.4$  Hz, 3 H), 8.27 (d,  $J=7.6$  Hz, 3 H), 8.22 (d,  $J=8.4$  Hz, 3 H), 7.76 (s, 3 H), 7.64–7.69 (m, 6 H), 7.57–7.61 (m, 3 H), 4.05 ppm (s, 9 H).

**4,4',4''-benzene-1,3,5-triyl-1,1',1''-trinaphthoic acid:** To a suspension of the tetramethyl intermediate (2.89 g, 4.58 mmol) in THF (40 mL) and MeOH (40 mL), was added 6 M NaOH (40 mL, 240 mM). The resulting mixture was refluxed overnight. After removal of the solvents, the residue was dissolved in water, and acidified with conc. HCl in an ice-water bath. The resulting precipitation was collected by filtration, washed with water and dried in vacuum at 343 K, affording the target compound in an almost quantitative yield.  $^1\text{H}$  NMR (600.1 MHz,  $[\text{D}_6]\text{DMSO}$ ):  $\delta=13.23$  (s, br, 3 H), 8.97–8.98 (m, 3 H), 8.22–8.23 (m, 6 H), 7.79 (d,  $J=7.8$  Hz, 3 H), 7.76 (s, 3 H), 7.67–7.72 ppm (m, 6 H);  $^{13}\text{C}$  NMR (75.4 MHz,  $[\text{D}_6]\text{DMSO}$ ):  $\delta=168.4$ , 142.8, 139.9, 131.1, 131.0, 130.4, 129.1, 127.8, 127.3, 126.7, 126.3, 125.9 ppm; selected FTIR (KBr):  $\tilde{\nu}=1689$ , 1577, 1514, 1464, 1425, 1375, 1282, 1248, 1194, 1140, 852, 795, 777, 723, 640, 430  $\text{cm}^{-1}$ .

**Synthesis and characterization of ZJNU-30:**  $\text{ZrCl}_4$  (5.0 mg, 21.4  $\mu\text{mol}$ , Alfa Aesar), the organic ligand (5.0 mg, 8.5  $\mu\text{mol}$ ), and benzoic acid (250 mg, 2.0 mmol, Energy Chemical) in DMA (1.5 mL) were ultrasonically dissolved in a 20 mL Teflon-lined autoclave. The mixture was heated at 403 K for 86 h. After the autoclave was cooled down to room temperature, polyhedron-shaped colorless crystals were collected by filtration. Yield: 4.2 mg, 32% based on the organic ligand. **ZJNU-30** can be best formulated as  $[\text{Zr}_9\text{O}_6(\text{OH})_6(\text{PhCOO})_6(\text{L})_4] \cdot 24\text{DMA}$  on the basis of single-crystal X-ray diffraction structure determination, TGA, and microanalysis. Selected FTIR (KBr):  $\tilde{\nu}=1645$ , 1600, 1560, 1512, 1410, 1371, 1265, 1188, 1012, 800, 779, 721, 648, 453  $\text{cm}^{-1}$ ; elemental analysis calcd (%) for  $\text{C}_{294}\text{H}_{336}\text{N}_{24}\text{O}_{72}\text{Zr}_9$ : C 57.15, H 5.48, N 5.44; found: C 56.70, H 5.50, N 5.23.

**Fitting of pure component isotherms:** The experimentally measured loadings for *n*-butane, *iso*-butane, 1-butene, *iso*-butene, *cis*-2-butene, *trans*-2-butene, and 1,3-butadiene at temperatures of

288, 298, and 308 K in **ZJNU-30a** were fitted with the DSLF isotherm model:

$$q = q_{A,\text{sat}} \frac{b_A p^{v_A}}{1 + b_A p^{v_A}} + q_{B,\text{sat}} \frac{b_B p^{v_B}}{1 + b_B p^{v_B}}$$

in which  $T$ -dependent parameters  $b_A$ , and  $b_B$  are:

$$b_A = b_{A0} \exp\left(\frac{E_A}{RT}\right); \quad b_B = b_{B0} \exp\left(\frac{E_B}{RT}\right)$$

The fitting parameters are provided in Table S2 in the Supporting Information.

**IAST calculations of adsorption selectivities and uptake capacities:** The selectivity of preferential adsorption of component 1 over component 2 in a mixture containing 1 and 2, perhaps in the presence of other components too, can be formally defined as:

$$S_{\text{ads}} = \frac{q_1/q_2}{p_1/p_2}$$

In this equation,  $q_1$  and  $q_2$  are the component loadings of the adsorbed phase in the mixture. These component loadings are also termed the uptake capacities. We calculate the values of  $q_1$  and  $q_2$  using the Ideal Adsorbed Solution Theory (IAST) of Myers and Prausnitz.<sup>[32]</sup>

## Acknowledgements

This work was supported by the National Natural Science Foundation of China (No. 21301156), the Natural Science Foundation of Zhejiang province, China (LR16B010001), and the Qianjiang Talents Project in Zhejiang province (Grant ZC304015017), and partly supported by the Welch Foundation (AX-1730).

**Keywords:** butene isomers • gas separation • metal-organic frameworks • tricarboxylate • zirconium

- [1] a) S. Kitagawa, *Angew. Chem. Int. Ed.* **2015**, *54*, 10686–10687; *Angew. Chem.* **2015**, *127*, 10834–10835; b) Y. He, B. Li, M. O’Keeffe, B. Chen, *Chem. Soc. Rev.* **2014**, *43*, 5618–5656; c) Y. He, W. Zhou, G. Qian, B. Chen, *Chem. Soc. Rev.* **2014**, *43*, 5657–5678; d) J. A. Mason, M. Veenstra, J. R. Long, *Chem. Sci.* **2014**, *5*, 32–51; e) Y. He, W. Zhou, T. Yildirim, B. Chen, *Energy Environ. Sci.* **2013**, *6*, 2735–2744; f) T. A. Makal, J.-R. Li, W. Lu, H.-C. Zhou, *Chem. Soc. Rev.* **2012**, *41*, 7761–7779; g) M. P. Suh, H. J. Park, T. K. Prasad, D.-W. Lim, *Chem. Rev.* **2012**, *112*, 782–835; h) Y. He, W. Zhou, R. Krishna, B. Chen, *Chem. Commun.* **2012**, *48*, 11813–11831; i) J. Sculley, D. Yuan, H.-C. Zhou, *Energy Environ. Sci.* **2011**, *4*, 2721–2735; j) L. J. Murray, M. Dincă, J. R. Long, *Chem. Soc. Rev.* **2009**, *38*, 1294–1314; k) A. Schoedel, Z. Ji, O. M. Yaghi, *Nat. Energy* **2016**, *1*, 16034.
- [2] a) Q. Wang, J. Bai, Z. Lu, Y. Pan, X. You, *Chem. Commun.* **2016**, *52*, 443–452; b) Z. R. Herm, E. D. Bloch, J. R. Long, *Chem. Mater.* **2014**, *26*, 323–338; c) J.-R. Li, J. Sculley, H.-C. Zhou, *Chem. Rev.* **2012**, *112*, 869–932; d) Y. He, R. Krishna, B. Chen, *Energy Environ. Sci.* **2012**, *5*, 9107–9120; e) K. Sumida, D. L. Rogow, J. A. Mason, T. M. McDonald, E. D. Bloch, Z. R. Herm, T.-H. Bae, J. R. Long, *Chem. Rev.* **2012**, *112*, 724–781; f) H. Wu, Q. Gong, D. H. Olson, J. Li, *Chem. Rev.* **2012**, *112*, 836–868; g) J.-R. Li, Y. Ma, M. C. McCarthy, J. Sculley, J. Yu, H.-K. Jeong, P. B. Balbuena, H.-C. Zhou, *Coord. Chem. Rev.* **2011**, *255*, 1791–1823; h) J.-R. Li, R. J. Kuppler, H.-C. Zhou, *Chem. Soc. Rev.* **2009**, *38*, 1477–1504.
- [3] a) M. Zhao, S. Ou, C.-D. Wu, *Acc. Chem. Res.* **2014**, *47*, 1199–1207; b) M. Yoon, R. Srirambalaji, K. Kim, *Chem. Rev.* **2012**, *112*, 1196–1231; c) G. Nickerl, A. Henschel, R. Grünker, K. Gedrich, S. Kaskel, *Chem. Ing. Tech.* **2011**, *83*, 90–103; d) Y. Liu, W. Xuan, Y. Cui, *Adv. Mater.* **2010**, *22*, 4112–4135; e) A. Corma, H. García, F. X. L. i. Xamena, *Chem. Rev.* **2010**, *110*, 4606–4655; f) J. Lee, O. K. Farha, J. Roberts, K. A. Scheidt, S. T. Nguyen, J. T. Hupp, *Chem. Soc. Rev.* **2009**, *38*, 1450–1459.
- [4] a) Z. Hu, B. J. Deibert, J. Li, *Chem. Soc. Rev.* **2014**, *43*, 5815–5840; b) Y. Cui, Y. Yue, G. Qian, B. Chen, *Chem. Rev.* **2012**, *112*, 1126–1162; c) L. E. Kreno, K. Leong, O. K. Farha, M. Allendorf, R. P. V. Duyne, J. T. Hupp, *Chem. Rev.* **2012**, *112*, 1105–1125.
- [5] a) S. C. Sahoo, T. Kundu, R. Banerjee, *J. Am. Chem. Soc.* **2011**, *133*, 17950–17958; b) J. A. Hurd, R. Vaidhyanathan, V. Thangadurai, C. I. Ratcliffe, I. L. Moudrakovski, G. K. H. Shimizu, *Nat. Chem.* **2009**, *1*, 705–710.
- [6] P. Horcajada, R. Gref, T. Baati, P. K. Allan, G. Maurin, P. Couvreur, G. Férey, R. E. Morris, C. Serre, *Chem. Rev.* **2012**, *112*, 1232–1268.
- [7] D. Yuan, D. Zhao, D. Sun, H.-C. Zhou, *Angew. Chem. Int. Ed.* **2010**, *49*, 5357–5361; *Angew. Chem.* **2010**, *122*, 5485–5489.
- [8] K. Koh, A. G. Wong-Foy, A. J. Matzger, *J. Am. Chem. Soc.* **2009**, *131*, 4184–4185.
- [9] H. Furukawa, N. Ko, Y. B. Go, N. Aratani, S. B. Choi, E. Choi, A. Ö. Yazaydin, R. Q. Snurr, M. O’Keeffe, J. Kim, O. M. Yaghi, *Science* **2010**, *329*, 424–428.
- [10] R. Grünker, V. Bon, P. Müller, U. Stoeck, S. Krause, U. Mueller, I. Senkovska, S. Kaskel, *Chem. Commun.* **2014**, *50*, 3450–3452.
- [11] O. K. Farha, I. Eryazici, N. C. Jeong, B. G. Hauser, C. E. Wilmer, A. A. Sarjeant, R. Q. Snurr, S. T. Nguyen, A. Ö. Yazaydin, J. T. Hupp, *J. Am. Chem. Soc.* **2012**, *134*, 15016–15021.
- [12] a) J. H. Cavka, S. Jakobsen, U. Olsbye, N. Guillou, C. Lamberti, S. Bordiga, K. P. Lillerud, *J. Am. Chem. Soc.* **2008**, *130*, 13850–13851; b) G. Férey, C. Serre, C. Mellot-Draznieks, F. Millange, S. Surblé, J. Dutour, I. Margiolaki, *Angew. Chem. Int. Ed.* **2004**, *43*, 6296–6301; *Angew. Chem.* **2004**, *116*, 6456–6461.
- [13] D. Ma, Y. Li, Z. Li, *Chem. Commun.* **2011**, *47*, 7377–7379.
- [14] W. Zhang, Y. Hu, J. Ge, H.-L. Jiang, S.-H. Yu, *J. Am. Chem. Soc.* **2014**, *136*, 16978–16981.
- [15] a) M. SK. S. Biswas, *CrystEngComm* **2016**, *18*, 3104–3113; b) G. Nickerl, I. Senkovska, S. Kaskel, *Chem. Commun.* **2015**, *51*, 2280–2282; c) K. Wang, H. Huang, W. Xue, D. Liu, X. Zhao, Y. Xiao, Z. Li, Q. Yang, L. Wang, C. Zhong, *CrystEngComm* **2015**, *17*, 3586–3590; d) B. Li, B. Gui, G. Hu, D. Yuan, C. Wang, *Inorg. Chem.* **2015**, *54*, 5139–5141; e) H. Fei, S. M. Cohen, *Chem. Commun.* **2014**, *50*, 4810–4812; f) L. Li, S. Tang, C. Wang, X. Lv, M. Jiang, H. Wu, X. Zhao, *Chem. Commun.* **2014**, *50*, 2304–2307; g) C. Wang, O. Volotskova, K. Lu, M. Ahmad, C. Sun, L. Xing, W. Lin, *J. Am. Chem. Soc.* **2014**, *136*, 6171–6174; h) J. M. Falkowski, T. Sawano, T. Zhang, G. Tsun, Y. Chen, J. V. Lockard, W. Lin, *J. Am. Chem. Soc.* **2014**, *136*, 5213–5216; i) Q. Yang, S. Vaesen, F. Ragon, A. D. Wiersum, D. Wu, A. Lago, T. Devic, C. Martineau, F. Taulelle, P. L. Llewellyn, H. Jobic, C. Zhong, C. Serre, G. D. Weireld, G. Maurin, *Angew. Chem. Int. Ed.* **2013**, *52*, 10316–10320; *Angew. Chem.* **2013**, *125*, 10506–10510; j) V. Bon, I. Senkovska, I. A. Baburin, S. Kaskel, *Cryst. Growth Des.* **2013**, *13*, 1231–1237; k) S. Biswas, J. Zhang, Z. Li, Y.-Y. Liu, M. Grzywa, L. Sun, D. Volkmer, P. V. D. Voort, *Dalton Trans.* **2013**, *42*, 4730–4737; l) K.-K. Yee, N. Reimer, J. Liu, S.-Y. Cheng, S.-M. Yiu, J. Weber, N. Stock, Z. Xu, *J. Am. Chem. Soc.* **2013**, *135*, 7795–7798; m) V. Guillerm, F. Ragon, M. Dan-Hardi, T. Devic, M. Vishnuvarthan, B. Campo, A. Vimont, G. Clet, Q. Yang, G. Maurin, G. Férey, A. Vittadini, S. Gross, C. Serre, *Angew. Chem. Int. Ed.* **2012**, *51*, 9267–9271; *Angew. Chem.* **2012**, *124*, 9401–9405; n) Y. Huang, W. Qin, Z. Li, Y. Li, *Dalton Trans.* **2012**, *41*, 9283–9285; o) A. Schaate, P. Roy, T. Preuß, S. J. Lohmeier, A. Godt, P. Behrens, *Chem. Eur. J.* **2011**, *17*, 9320–9325.
- [16] a) L. Xu, Y.-P. Luo, L. Sun, Y. Xu, Z.-S. Cai, M. Fang, R.-X. Yuan, H.-B. Du, *Chem. Eur. J.* **2016**, *22*, 6268–6276; b) H. Cui, Y. Wang, Y. Wang, Y. Fan, L. Zhang, C.-Y. Su, *CrystEngComm* **2016**, *18*, 2203–2209; c) S. B. Kalidindi, S. Nayak, M. E. Briggs, S. Jansat, A. P. Katsoulidis, G. J. Miller, J. E. Warren, D. Antypov, F. Corà, B. Slater, M. R. Prestly, C. M. -Gastaldo, M. J. Rosseinsky, *Angew. Chem. Int. Ed.* **2015**, *54*, 221–226; *Angew. Chem.* **2015**, *127*, 223–228; d) S. Wang, J. Wang, W. Cheng, X. Yang, Z. Zhang, Y. Xu, H. Liu, Y. Wu, M. Fang, *Dalton Trans.* **2015**, *44*, 8049–8061; e) Q. Zhang, J. Su, D. Feng, Z. Wei, X. Zou, H.-C. Zhou, *J. Am. Chem. Soc.* **2015**, *137*, 10064–10067; f) R. Zou, X. Ren, F. Huang, Y. Zhao, J. Liu, X. Jing, F. Liao, Y. Wang, J. Lin, R. Zou, J. Sun, *J. Mater. Chem. A* **2015**, *3*, 23493–23500; g) D. Feng, H.-L. Jiang, Y.-P. Chen, Z.-Y. Gu, Z. Wei, H.-C. Zhou, *Inorg.*

- Chem.* **2013**, *52*, 12661–12667; h) H.-L. Jiang, D. Feng, K. Wang, Z.-Y. Gu, Z. Wei, Y.-P. Chen, H.-C. Zhou, *J. Am. Chem. Soc.* **2013**, *135*, 13934–13938; i) M. Zhang, Y.-P. Chen, M. Bosch, T. Gentle, III., K. Wang, D. Feng, Z. U. Wang, H.-C. Zhou, *Angew. Chem. Int. Ed.* **2014**, *53*, 815–818; *Angew. Chem.* **2014**, *126*, 834–837; j) Y. Chen, T. Hoang, S. Ma, *Inorg. Chem.* **2012**, *51*, 12600–12602; k) D. Feng, Z.-Y. Gu, J.-R. Li, H.-L. Jiang, Z. Wei, H.-C. Zhou, *Angew. Chem. Int. Ed.* **2012**, *51*, 10307–10310; *Angew. Chem.* **2012**, *124*, 10453–10456; l) W. Morris, B. Voloskiy, S. Demir, F. Gándara, P. L. McGrier, H. Furukawa, D. Cascio, J. F. Stoddart, O. M. Yaghi, *Inorg. Chem.* **2012**, *51*, 6443–6445.
- [17] a) H. Furukawa, F. Gándara, Y.-B. Zhang, J. Jiang, W. L. Queen, M. R. Hudson, O. M. Yaghi, *J. Am. Chem. Soc.* **2014**, *136*, 4369–4381; b) R. Wang, Z. Wang, Y. Xu, F. Dai, L. Zhang, D. Sun, *Inorg. Chem.* **2014**, *53*, 7086–7088.
- [18] a) Y.-B. Zhang, H. Furukawa, N. Ko, W. Nie, H. J. Park, S. Okajima, K. E. Cordova, H. Deng, J. Kim, O. M. Yaghi, *J. Am. Chem. Soc.* **2015**, *137*, 2641–2650; b) Y. He, H. Furukawa, C. Wu, M. O'Keeffe, R. Krishna, B. Chen, *Chem. Commun.* **2013**, *49*, 6773–6775; c) Y. He, Z. Zhang, S. Xiang, F. R. Fronczeck, R. Krishna, B. Chen, *Chem. Commun.* **2012**, *48*, 6493–6495; d) K. Gedrich, I. Senkovska, N. Klein, U. Stoeck, A. Henschel, M. R. Lohe, I. A. Baburin, U. Mueller, S. Kaskel, *Angew. Chem. Int. Ed.* **2010**, *49*, 8489–8492; *Angew. Chem.* **2010**, *122*, 8667–8670; e) D. Sun, S. Ma, Y. Ke, D. J. Collins, H.-C. Zhou, *J. Am. Chem. Soc.* **2006**, *128*, 3896–3897; f) H. K. Chae, D. Y. Siberio-Pérez, J. Kim, Y. Go, M. Eddaoudi, A. J. Matzger, M. O'Keeffe, O. M. Yaghi, *Nature* **2004**, *427*, 523–527; g) B. Chen, M. Eddaoudi, S. T. Hyde, M. O'Keeffe, O. M. Yaghi, *Science* **2001**, *291*, 1021–1023.
- [19] Y. Bai, Y. Dou, L.-H. Xie, W. Rutledge, J.-R. Li, H.-C. Zhou, *Chem. Soc. Rev.* **2016**, *45*, 2327–2367.
- [20] A. L. Spek, *Acta Crystallogr. Sect. D* **2009**, *65*, 148–155.
- [21] J. Rouquerol, P. Llewellyn, F. Rouquerol, *Stud. Surf. Sci. Catal.* **2007**, *160*, 49–56.
- [22] K. S. Walton, R. Q. Snurr, *J. Am. Chem. Soc.* **2007**, *129*, 8552–8556.
- [23] a) R. Krishna, *Phys. Chem. Chem. Phys.* **2015**, *17*, 39–59; b) H. Kim, Y. Jung, *J. Phys. Chem. Lett.* **2014**, *5*, 440–446.
- [24] a) B. Tijsebaert, C. Varszegi, H. Gies, F.-S. Xiao, X. Bao, T. Tatsumi, U. Müller, D. D. Vos, *Chem. Commun.* **2008**, 2480–2482; b) M. Hartmann, S. Kunz, D. Himsl, O. Tangermann, *Langmuir* **2008**, *24*, 8634–8642; c) M. Palomino, A. Cantín, A. Corma, S. Leiva, F. Rey, S. Valencia, *Chem. Commun.* **2007**, 1233–1235; d) A. Takahashi, R. T. Yang, C. L. Munson, D. Chinn, *Langmuir* **2001**, *17*, 8405–8413; e) W. Zhu, F. Kapteijn, J. A. Moulijn, J. C. Jansen, *Phys. Chem. Chem. Phys.* **2000**, *2*, 1773–1779; f) J. Padin, R. T. Yang, C. L. Munson, *Ind. Eng. Chem. Res.* **1999**, *38*, 3614–3621.
- [25] J. van den Bergh, C. Güçüyener, E. A. Pidko, E. J. M. Hensen, J. Gascon, F. Kapteijn, *Chem. Eur. J.* **2011**, *17*, 8832–8840.
- [26] C. Chmelik, J. Kärger, M. Wiebecke, J. Caro, J. M. v. Baten, R. Krishna, *Mesoporous Mesoporous Mater.* **2009**, *117*, 22–32.
- [27] R. Babarao, Y. H. Tong, J. Jiang, *J. Phys. Chem. B* **2009**, *113*, 9129–9136.
- [28] L. Zhang, Q. Wang, T. Wu, Y.-C. Liu, *Chem. Eur. J.* **2007**, *13*, 6387–6396.
- [29] a) F. Wang, W. Wang, S. Huang, J. Teng, Z. Xie, *Chin. J. Chem. Eng.* **2007**, *15*, 376–386; b) M.-G. Olivier, K. Berlier, J. Bougard, *J. Chem. Eng. Data* **1994**, *39*, 774–776; c) M.-G. Olivier, K. Berlier, R. Jadot, *J. Chem. Eng. Data* **1994**, *39*, 770–773; d) S. H. Hyun, R. P. Danner, *J. Chem. Eng. Data* **1982**, *27*, 196–200.
- [30] R. Krishna, *RSC Adv.* **2015**, *5*, 52269–52295.
- [31] G. M. Sheldrick, *Acta Crystallogr. Sect. A* **2008**, *64*, 112–122.
- [32] A. L. Myers, J. M. Prausnitz, *AIChE J.* **1965**, *11*, 121–127.

Received: June 16, 2016

Published online on September 6, 2016

# CHEMISTRY

## A European Journal

### Supporting Information

#### **A Porous Zirconium-Based Metal-Organic Framework with the Potential for the Separation of Butene Isomers**

Huimin Liu,<sup>[a]</sup> Yabing He,<sup>\*[a]</sup> Jingjing Jiao,<sup>[a]</sup> Dongjie Bai,<sup>[a]</sup> De-li Chen,<sup>[b]</sup> Rajamani Krishna,<sup>\*[c]</sup> and Banglin Chen<sup>\*[a, d]</sup>

chem\_201602892\_sm\_miscellaneous\_information.pdf

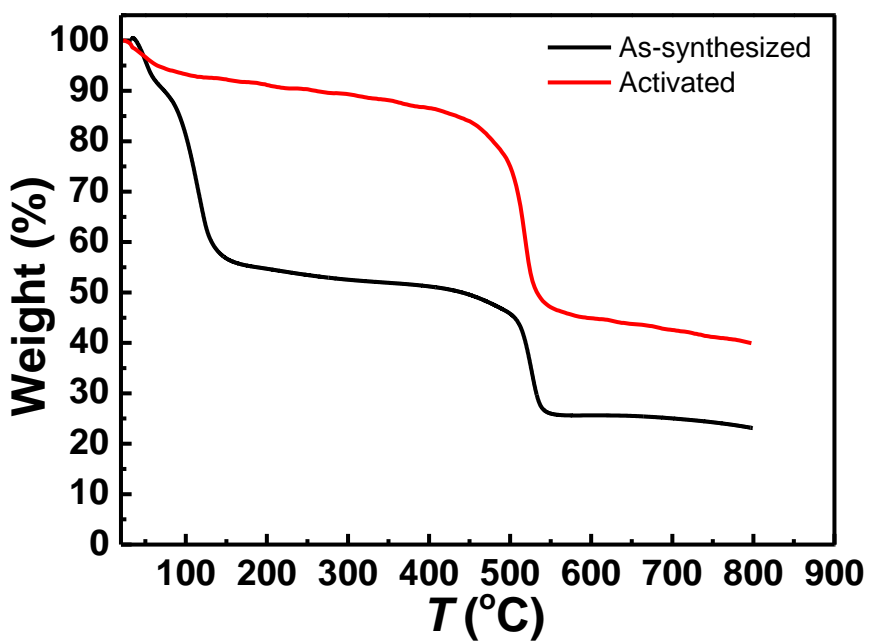


**Fig. S1** TGA curves of the as-synthesized **ZJNU-30** and activated **ZJNU-30a** under  $\text{N}_2$  atmosphere with a heating rate of  $5 \text{ K min}^{-1}$ .

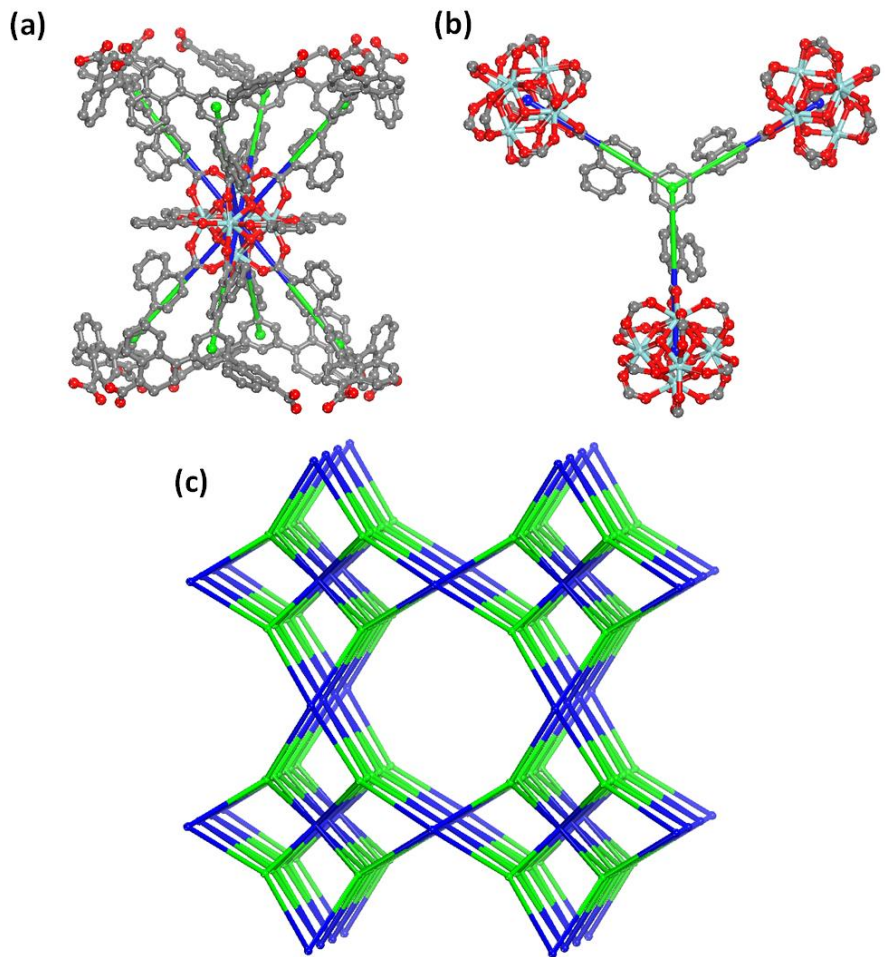
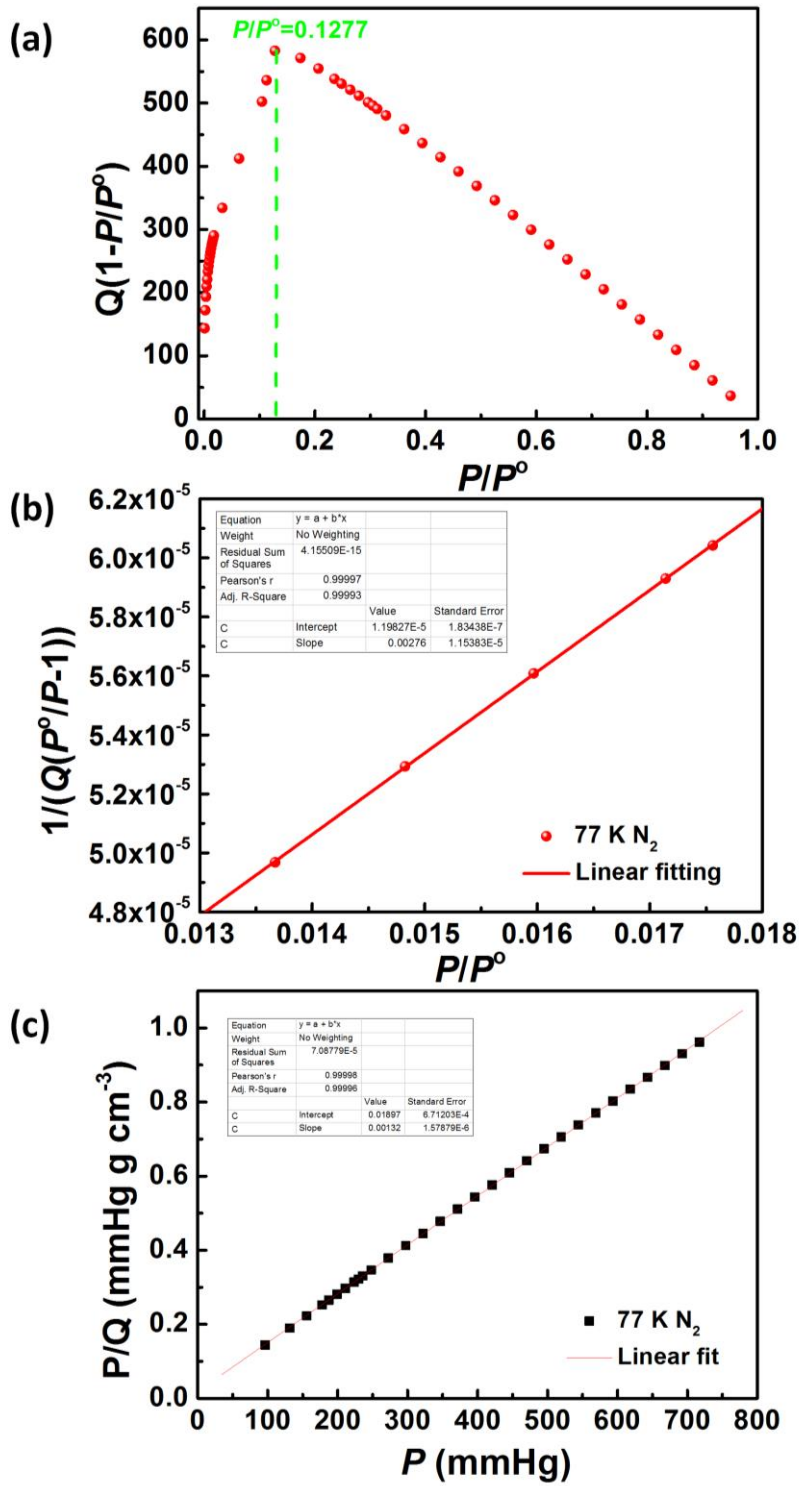


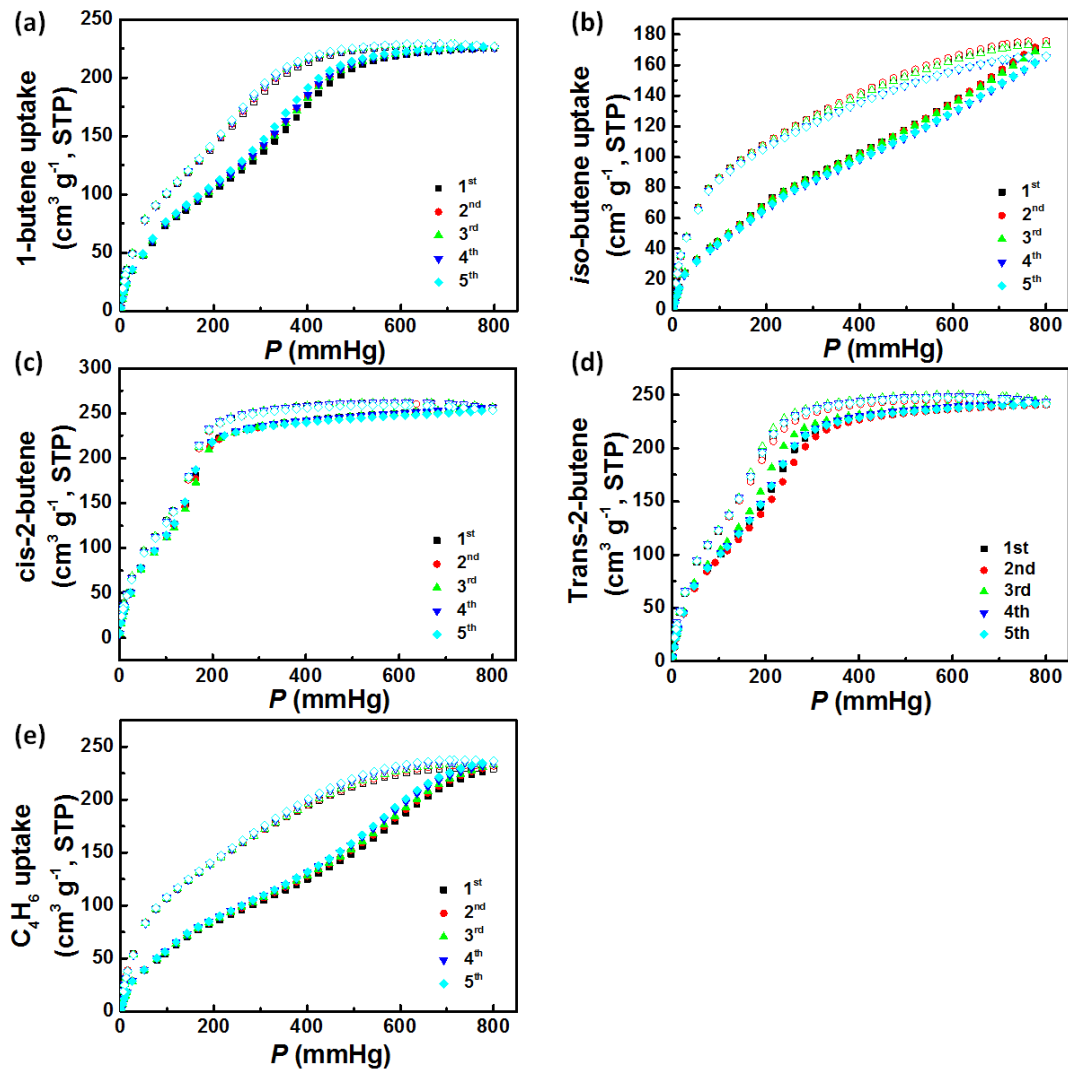
**Fig. S2** (a) View of the 8-connected SBU; (b) view of the 3-connected ligand; (c) schematic representation of (3,8)-connected net with the point symbol of  $\{4^8 \cdot 6^4 \cdot 8^{12} \cdot 10^4\}$ .



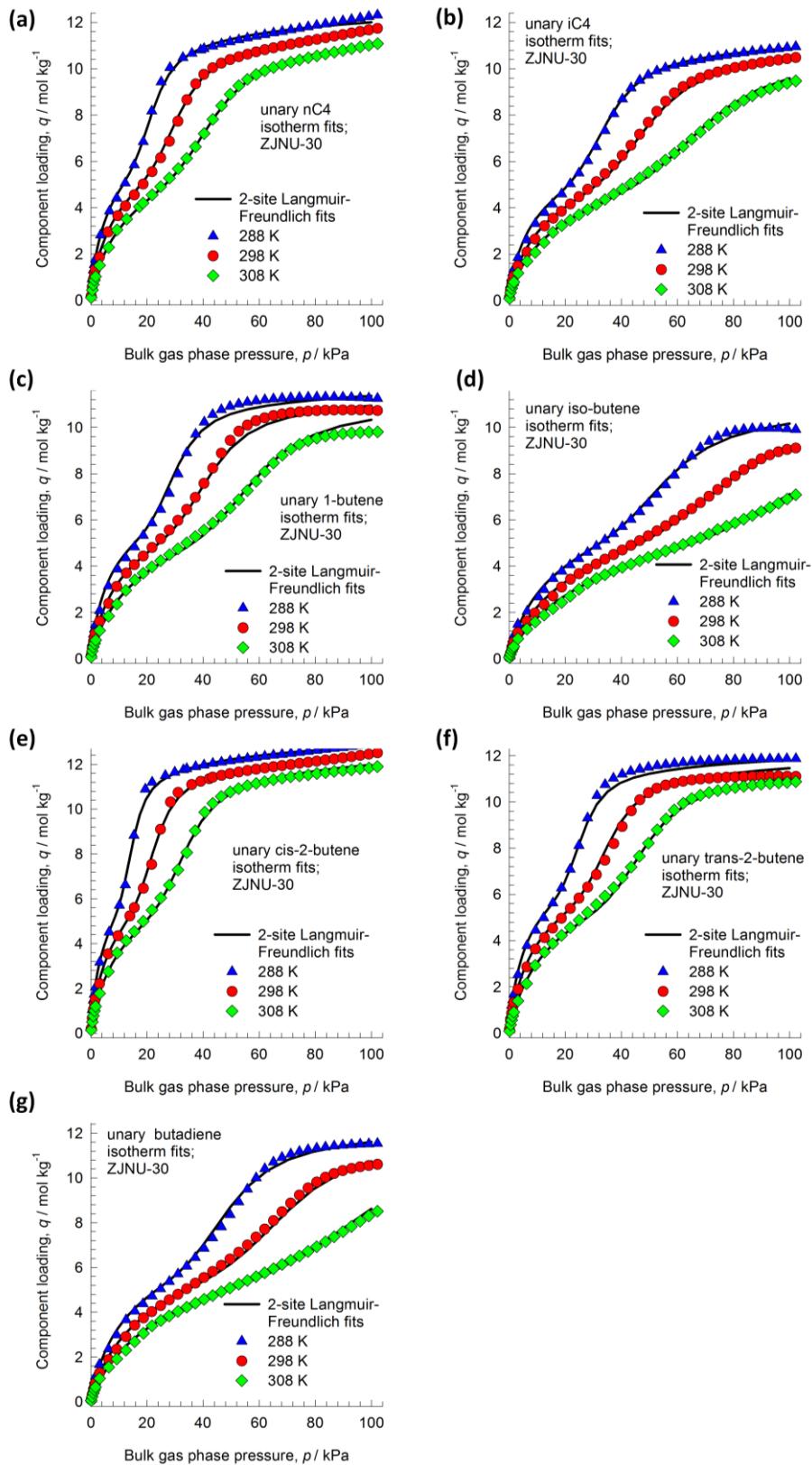
$$S_{\text{BET}} = 1/(0.00276 + 0.0000119827)/22414 \times 6.023 \times 10^{23} \times 0.162 \times 10^{-18} = 1570.4 \text{ m}^2 \text{ g}^{-1}$$

$$S_{\text{Langmuir}} = (1/0.00132)/22414 \times 6.023 \times 10^{23} \times 0.162 \times 10^{-18} = 3297.9 \text{ m}^2 \text{ g}^{-1}$$

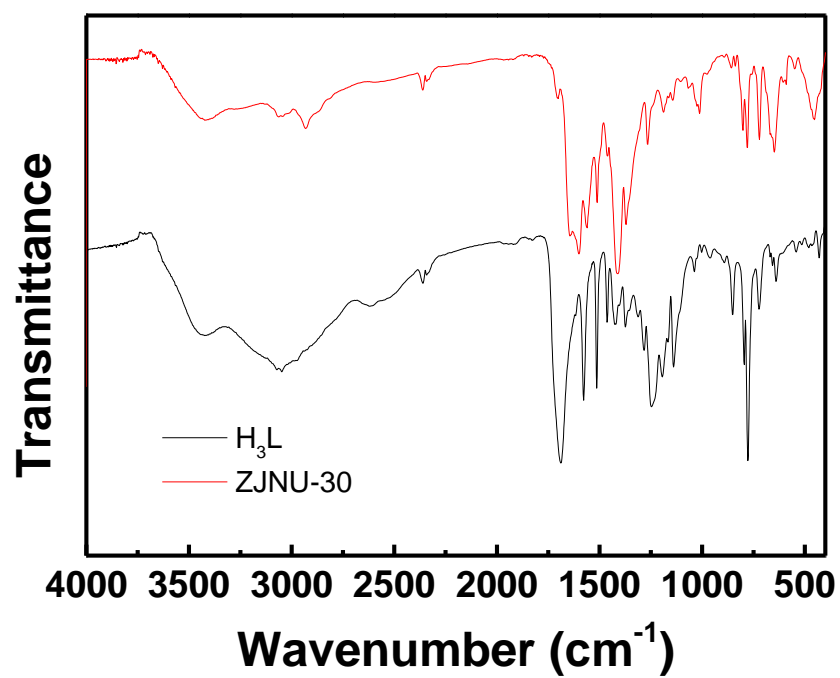
**Fig. S3** The consistency plot (a), BET (b) and Langmuir (c) fitting for **ZJNU-30a**.



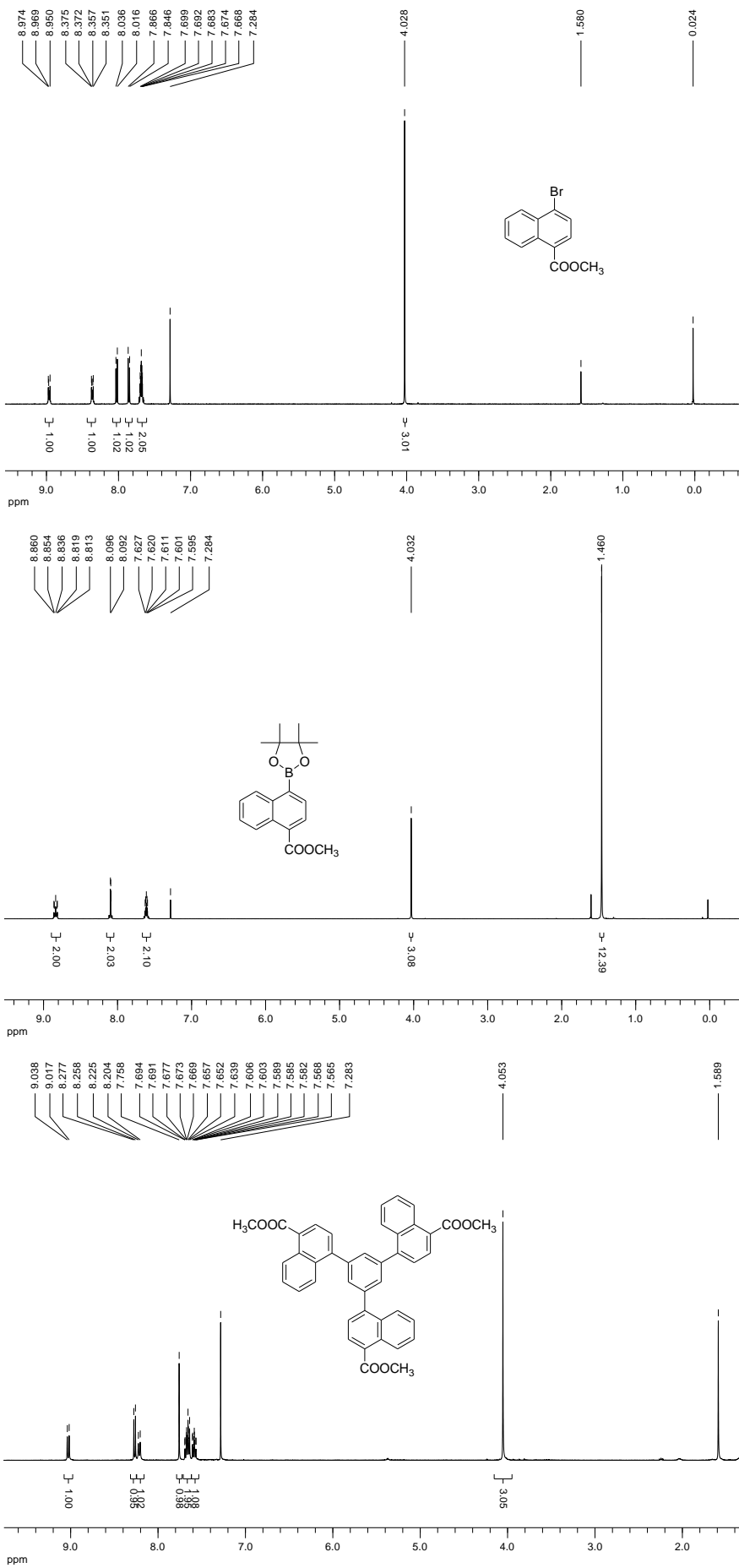
**Fig. S4** Five cycles of 1-butene (a), iso-butene (b), cis-2-butene (c), trans-2-butene (d) and 1,3-butadiene (e) gas adsorptions in **ZJNU-30a**. Note that the reactivation process was applied between each cycle, which was achieved by heating the sample at 333 K until the degassed rate reached  $3 \mu\text{mHg min}^{-1}$ .



**Fig. S5** Comparison of component loadings for *n*-butane (a), *iso*-butane (b), 1-butene (c), *iso*-butene (d), *cis*-2-butene (e), *trans*-2-butene (f), and 1,3-butadiene (g) at temperatures of 288 K, 298 K and 308 K in **ZJNU-30a** with the isotherm fits.



**Fig. S6** FTIR spectra of the organic ligand  $H_3L$  (black) and the as-synthesized **ZJNU-30** (red).



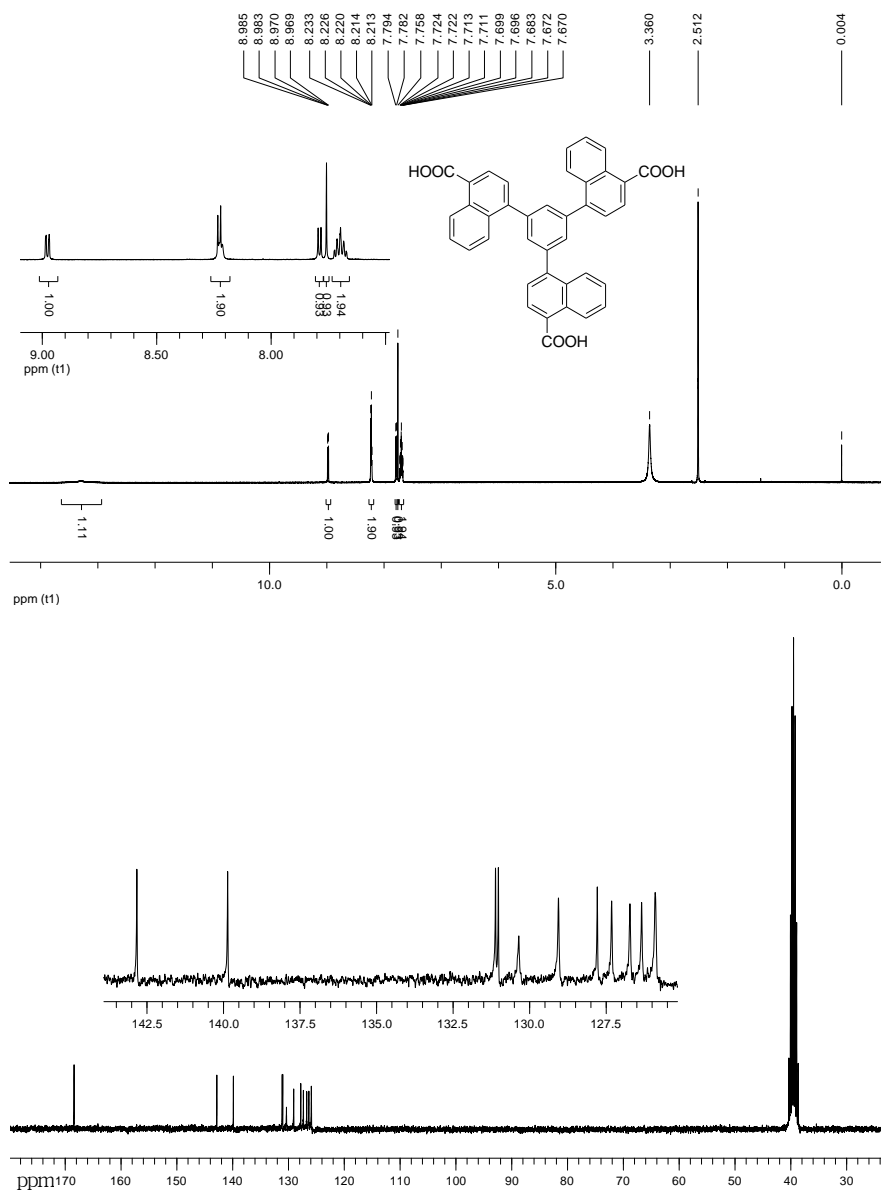


**Fig. S7**  $^1\text{H}$  and  $^{13}\text{C}$  NMR spectra

**Table S1** BET surface areas and pore volumes of the reported Zr-MOFs

Zr-MOFs	$V_p$ (cm <sup>3</sup> g <sup>-1</sup> )	BET (m <sup>2</sup> g <sup>-1</sup> )	Ref.
NU-1103	2.91	6550	[1]
NU-1104	2.79	6230	[1]
NU-1105	2.17	3700	[2]
NU-1102	2.00	4830	[1]
NU-1101	1.72	4340	[1]
PCN-222(Fe)	1.56	2200	[3]
NU-1100	1.53	4060	[4]
NU-1000	1.4	2320	[5]
ZJNU-30	1.15	1570	This work
DUT-51(Zr)	1.08	2335	[6]
UiO(bpdc)	1.057	2646	[7]
PCN-221	0.76	1936	[8]
UiO-66(dhtz)	0.73	1632	[9]
Zr <sub>6</sub> O <sub>4</sub> (OH) <sub>4</sub> (TCPS) <sub>2</sub> (OH) <sub>4</sub> (H <sub>2</sub> O) <sub>4</sub>	0.69	1402	[10]
Zr <sub>6</sub> O <sub>4</sub> (OH) <sub>4</sub> (OH) <sub>6</sub> (H <sub>2</sub> O) <sub>6</sub> (BTB) <sub>2</sub>	0.27	613	[11]
PCN-521	NA	3411	[12]
MOF-525	NA	2620	[13]
PCN-128W	NA	2532	[14]
MOF-545	NA	2260	[13]
UiO-66	NA	1580	[15]
MOF-535	NA	1120	[13]

**Table S2** Comparison of C<sub>4</sub>-hydrocarbon adsorption data in the reported MOFs

Adsorptive	MOFs	T (K)	P (kPa)	Uptake (mol kg <sup>-1</sup> )	Ref.
<i>n</i> -butane	DUT-6(Zn)	293		18.9 <sup>a</sup>	[16]
	DUT-9(Ni)	293		12.0 <sup>a</sup>	[17]
	<b>ZJNU-30a</b>	298	100	11.8	This work
	MIL-101	293		11.2 <sup>a</sup>	[18]
	ZJNU-80a	298	100	7.93	[19]
	DUT-8(Ni)	293		6.0 <sup>a</sup>	[20]
	MIL-53(Cr)	303	100	3.9	[21]
	Cu-BTC <sup>b</sup>	293		3.7 <sup>a</sup>	[18]
	Cu-Me <sub>2</sub> trz-pba <sup>c</sup>	313	100	3.4	[22]
	MIL-53(Fe)	303	100	2.8	[21]
	ZIF-7	298	100	2.6	[23]
	Y-fum <sup>d</sup>	293	100	2.0	[24]
	Eu-1,4-NDC <sup>e</sup>	298	100	1.56	[25]
<i>iso</i> -butane	<b>ZJNU-30a</b>	298	100	10.5	This work
	ZJNU-80a	298	100	7.5	[19]
	Zn-DABCO	294	100	6.4	[26]
	MIL-100(Fe)	323	100	5.0	[27]
	Cu-BTC	303	3	4.3	[28]
	Cu-Me <sub>2</sub> trz-pba <sup>c</sup>	313	100	3.6	[22]
<i>iso</i> -butene	<b>ZJNU-30a</b>	298	100	9.14	This work
	ZJNU-80a	298	100	6.8	[19]
	Cu-BTC <sup>b</sup>	303	3	5.1	[28]
	Cu-Me <sub>2</sub> trz-pba <sup>c</sup>	313	100	4.0	[22]
1-butene	<b>ZJNU-30a</b>	298	100	10.7	This work
	ZJNU-80a	298	100	8.35	[19]
	Cu-Me <sub>2</sub> trz-pba <sup>c</sup>	313	100	3.8	[22]
	ZIF-7	298	100	2.13	[23]
<i>cis</i> -2-butene	<b>ZJNU-30a</b>	298	100	12.57	This work
	ZJNU-80a	298	100	9.16	[19]
	ZIF-7	298	100	2.58	[23]
<i>trans</i> -2-butene	<b>ZJNU-30a</b>	298	100	11.10	This work
	ZJNU-80a	298	100	8.66	[19]
	ZIF-7	298	100	2.7	[23]
1,3-butadiene	<b>ZJNU-30a</b>	298	100	10.63	This work

<sup>a</sup> Saturation capacity; <sup>b</sup> BTC = benzene-1,3,5-tricarboxylate; <sup>c</sup> Me<sub>2</sub>trz-pba = 4-(3,5-dimethyl-4H-1,2,4-triazol-4-yl)benzoate; <sup>d</sup> fum = fumarate; <sup>e</sup> 1,4-NDC = 1,4-naphthalenedicarboxylate

**Table S3** Dual-site Langmuir-Freundlich fitting parameters for *n*-butane, *iso*-butane, 1-butene, *iso*-butene, *cis*-2-butene, *trans*-2-butene, and 1,3-butadiene in **ZJNU-30a**.

	Site A				Site B			
	$q_{A,\text{sat}}$ mol kg <sup>-1</sup>	$b_{A0}$ Pa <sup>-<math>\nu_A</math></sup>	$E_A$ kJ mol <sup>-1</sup>	$\nu_A$ dimensionless	$q_{B,\text{sat}}$ mol kg <sup>-1</sup>	$b_{B0}$ Pa <sup>-<math>\nu_B</math></sup>	$E_B$ kJ mol <sup>-1</sup>	$\nu_B$ dimensionless
<i>n</i> -butane	9.1	$8.4 \times 10^{-9}$	27	0.8	4.1	$8.84 \times 10^{-54}$	149	6
<i>iso</i> -butane	8	$1.77 \times 10^{-8}$	24.6	0.8	4.2	$6.9 \times 10^{-54}$	147	5.84
1-butene	8.1	$1.39 \times 10^{-9}$	30	0.86	4.2	$1.71 \times 10^{-55}$	149	6.2
<i>iso</i> -butene	8.5	$1.45 \times 10^{-8}$	23	0.84	3.7	$4.47 \times 10^{-54}$	140	5.9
<i>cis</i> -2-butene	9	$4.23 \times 10^{-9}$	28.5	0.84	4.6	$3.81 \times 10^{-62}$	194	6.3
<i>trans</i> -2-butene	8.4	$1.4 \times 10^{-9}$	30	0.88	4.2	$3.64 \times 10^{-59}$	157	6.8
1,3-butadiene	9	$1.58 \times 10^{-8}$	23	0.85	4.4	$6.06 \times 10^{-58}$	158	6.1

**Table S4** Crystal data and structure refinement for **ZJNU-30**.

Compounds	<b>ZJNU-30</b>
Empirical formula	C <sub>66</sub> H <sub>40</sub> O <sub>16</sub> Zr <sub>3</sub>
Formula weight	1362.64
Wavelength (Å)	0.71069
Crystal system	Cubic
Space group	Pm-3m
Unit cell dimensions	$a = 28.345(5)$ Å $b = 28.345(5)$ Å $c = 28.345(5)$ Å $\alpha = 90.000(5)^\circ$ $\beta = 90.000(5)^\circ$ $\gamma = 90.000(5)^\circ$
Volume (Å <sup>3</sup> )	22773(7)
Z	6
Calculated density (g cm <sup>-3</sup> )	0.596
Absorption coefficient (mm <sup>-1</sup> )	0.230
$F(000)$	4104
$\theta$ range for data collection (°)	3.13 to 27.48
Limiting indices	-24 ≤ $h$ ≤ 36, -33 ≤ $k$ ≤ 27, -36 ≤ $l$ ≤ 36
Reflections collected / unique	108819 / 4953
$R_{\text{int}}$	0.0697
Completeness to $\theta = 25.02$	98.6%
Max. and min. transmission	0.9864 and 0.9686
Refinement method	Full-matrix least-squares on $F^2$
Data / restraints / parameters	4953 / 37 / 136
Goodness-of-fit on $F^2$	1.004
Final $R$ indices [ $I > 2\sigma(I)$ ]	$R_1 = 0.0748$ , $wR_2 = 0.1842$
$R$ indices (all data)	$R_1 = 0.1630$ , $wR_2 = 0.2157$
Largest diff. peak and hole (e.Å <sup>-3</sup> )	0.547 and -0.339
CCDC	1446516

## Reference

- [1] T. C. Wang, W. Bury, D. A. Gómez-Gualdrón, N. A. Vermeulen, J. E. Mondloch, P. Deria, K. Zhang, P. Z. Moghadam, A. A. Sarjeant, R. Q. Snurr, J. F. Stoddart, J. T. Hupp, O. K. Farha, *J. Am. Chem. Soc.* **2015**, *137*, 3585-3591.
- [2] P. Deria, D. A. Gómez-Gualdrón, W. Bury, H. T. Schaef, T. C. Wang, P. K. Thallapally, A. A. Sarjeant, R. Q. Snurr, J. T. Hupp, O. K. Farha, *J. Am. Chem. Soc.* **2015**, *137*, 13183-13190.
- [3] D. Feng, Z.-Y. Gu, J.-R. Li, H.-L. Jiang, Z. Wei, H.-C. Zhou, *Angew. Chem. Int. Ed.* **2012**, *51*, 10307-10310.
- [4] O. V. Gutov, W. Bury, D. A. Gomez-Gualdrón, V. Krungleviciute, D. Fairen-Jimenez, J. E. Mondloch, A. A. Sarjeant, S. S. Al-Juaid, R. Q. Snurr, J. T. Hupp, T. Yildirim, O. K. Farha, *Chem. Eur. J.* **2014**, *20*, 12389-12393.
- [5] J. E. Mondloch, W. Bury, D. Fairen-Jimenez, S. Kwon, E. J. DeMarco, M. H. Weston, A. A. Sarjeant, S. T. Nguyen, P. C. Stair, R. Q. Snurr, O. K. Farha, J. T. Hupp, *J. Am. Chem. Soc.* **2013**, *135*, 10294-10297.
- [6] V. Bon, V. Senkovskyy, I. Senkovska, S. Kaskel, *Chem. Commun.* **2012**, *48*, 8407-8409.
- [7] L. Li, S. Tang, C. Wang, X. Lv, M. Jiang, H. Wu, X. Zhao, *Chem. Commun.* **2014**, *50*, 2304-2307.
- [8] D. Feng, H.-L. Jiang, Y.-P. Chen, Z.-Y. Gu, Z. Wei, H.-C. Zhou, *Inorg. Chem.* **2013**, *52*, 12661-12667.
- [9] G. Nickerl, I. Senkovska, S. Kaskel, *Chem. Commun.* **2015**, *51*, 2280-2282.
- [10] S. Wang, J. Wang, W. Cheng, X. Yang, Z. Zhang, Y. Xu, H. Liu, Y. Wu, M. Fang, *Dalton Trans.* **2015**, *44*, 8049-8061.
- [11] R. Wang, Z. Wang, Y. Xu, F. Dai, L. Zhang, D. Sun, *Inorg. Chem.* **2014**, *53*, 7086-7088.
- [12] M. Zhang, Y.-P. Chen, M. Bosch, T. G. III, K. Wang, D. Feng, Z. U. Wang, H.-C. Zhou, *Angew. Chem. Int. Ed.* **2013**, *52*, 815-818
- [13] W. Morris, B. Voloskiy, S. Demir, F. Gándara, P. L. McGrier, H. Furukawa, D. Cascio, J. F. Stoddart, O. M. Yaghi, *Inorg. Chem.* **2012**, *51*, 6443-6445.
- [14] Q. Zhang, J. Su, D. Feng, Z. Wei, X. Zou, H.-C. Zhou, *J. Am. Chem. Soc.* **2015**, *137*, 10064-10067.
- [15] aJ. H. Cavka, S. Jakobsen, U. Olsbye, N. Guillou, C. Lamberti, S. Bordiga, K. P. Lillerud, *J. Am. Chem. Soc.* **2008**, *130*, 13850-13851; bM. J. Katz, Z. J. Brown, Y. J. Colón, P. W. Siu, K. A. Scheidt, R. Q. Snurr, J. T. Hupp, O. K. Farha, *Chem. Commun.* **2013**, *49*, 9449-9451.
- [16] N. Klein, I. Senkovska, K. Gedrich, U. Stoeck, A. Henschel, U. Mueller, S. Kaskel, *Angew. Chem. Int. Ed.* **2009**, *48*, 9954-9957.
- [17] K. Gedrich, I. Senkovska, N. Klein, U. Stoeck, A. Henschel, M. R. Lohe, I. A. Baburin, U. Mueller, S. Kaskel, *Angew. Chem. Int. Ed.* **2010**, *49*, 8489-8492.
- [18] N. Klein, A. Henschel, S. Kaskel, *Microporous Mesoporous Mater.* **2010**, *129*, 238-242.
- [19] J. Jiao, H. Liu, D. Bai, Y. He, *Inorg. Chem.* **2016**, *55*, 3974-3979.

- [20] N. Klein, C. Herzog, M. Sabo, I. Senkovska, J. Getzschmann, S. Paasch, M. R. Lohe, E. Brunner, S. Kaskel, *Phys. Chem. Chem. Phys.* **2010**, *12*, 11778-11784.
- [21] P. L. Llewellyn, P. Horcajada, G. Maurin, T. Devic, N. Rosenbach, S. Bourrelly, C. Serre, D. Vincent, S. Loera-Serna, Y. Filinchuk, G. Férey, *J. Am. Chem. Soc.* **2009**, *131*, 13002-13008.
- [22] M. Lange, M. Kobalz, J. Bergmann, D. Lässig, J. Lincke, J. Möllmer, A. Möller, J. Hofmann, H. Krautscheid, R. Staudt, R. Gläser, *J. Mater. Chem. A* **2014**, *2*, 8075-8085.
- [23] J. v. d. Bergh, C. Güçüyener, E. A. Pidko, E. J. M. Hensen, J. Gascon, F. Kapteijn, *Chem. Eur. J.* **2011**, *17*, 8832-8840.
- [24] A. H. Assen, Y. Belmabkhout, K. Adil, P. M. Bhatt, D.-X. Xue, H. Jiang, M. Eddaoudi, *Angew. Chem. Int. Ed.* **2015**, *54*, 14353-14358.
- [25] D.-X. Xue, Y. Belmabkhout, O. Shekhah, H. Jiang, K. Adil, A. J. Cairns, M. Eddaoudi, *J. Am. Chem. Soc.* **2015**, *137*, 5034-5040.
- [26] Y. He, W. Zhou, G. Qian, B. Chen, *Chem. Soc. Rev.* **2014**, *43*, 5657-5678.
- [27] M. G. Plaza, A. M. Ribeiro, A. Ferreira, J. C. Santos, Y. K. Hwang, Y.-K. Seo, U.-H. Lee, J.-S. Chang, J. M. Loureiro, A. E. Rodrigues, *Microporous Mesoporous Mater.* **2012**, *153*, 178-190.
- [28] M. Hartmann, S. Kunz, D. Himsl, O. Tangermann, *Langmuir* **2008**, *24*, 8634-8642.